Isomorphism between the electro-elastic modeling of the spin transition and Ising-like model with competing interactions: Elastic generation of self-organized spin states

Mamadou Ndiaye, Yogendra Singh, Houcem Fourati, Mouhamadou Sy, Bassirou Lo, Kamel Boukheddaden

Isomorphism between the Electro-Elastic Modelling of the Spin Transition and Ising-like Model with Competing Interactions: Elastic Generation of Self-Organized Spin States

Mamadou Ndiaye[1,2], Yogendra Singh[1], Houcem Fourati[1,3], Mouhamadou Sy[4], Bassirou Lo[2] and Kamel Boukheddaden[1,a)]

[1]*Université Paris-Saclay, UVSQ, CNRS, GEMaC, 45 Avenue des Etats Unis, 78035 Versailles, France*
[2]*Université Cheikh Anta Diop de Dakar, BP 5005, Fann, Dakar, Sénégal*
[3]*Laboratoire de Physique Appliquée, Université de Sfax, FSS, Route de Soukra km 3.5, 3000, Sfax, Tunisie*
[4]*Université Assane Seck de Ziguinchor, BP 523, Ziguinchor, Sénégal*

[a)] Corresponding author: kamel.boukheddaden@uvsq.fr

ABSTRACT:

Elastic modelling of spin-crossover material has boomed remarkably these last years. Among these models, the electro-elastic model combining spin and lattice degrees of freedom showed good abilities of fair description of the thermodynamics and spin-crossover solids. In the present work, we explore a new treatment of this model based on a homogeneous description of the lattice spacing with well separate relaxation timescales for the lattice and spin state degrees of freedom. This description is analogous to the Born-Oppenheimer approximation and allows analytic treatment of the elastic part of the model, thus simplifying considerably the model resolution. As a result, we have been able to demonstrate the equivalence between the genuine electro-elastic model and an Ising-like Hamiltonian with-competing long-range ferro-like and short-range (nearest neighbors and next-nearest neighbors along diagonals) antiferro-like interactions, whose relationship with the high-spin to low-spin misfit elastic energy has been established. This model generates intrinsic elastic frustration in the lattice, which leads to a rich variety of hysteretic first-order transitions made of one- two-, three- or four-steps behaviors. Complex self-organizations of the spin states are evidenced in the plateau regions in form of checkerboard-like, stripes-like patterns, constituted of alternate high-spin and low-spin ferro-like stripes or alternate ferro high-spin (or low-spin) and antiferro-like chains, as well labyrinth structures.

I. INTRODUCTION

Spin-crossover (SCO) compounds are extensively studied in the literature due to their rich physical properties covering optics [1-4], spintronics [5-11], magnetism [12-15], elasticity [16-18], and statistical mechanics [19, 20]. SCO materials are molecular solids containing a metallic central atom surrounded by ligands in an octahedral symmetry. Fe(II)-based SCO complexes exhibit two spin states, a paramagnetic high-spin $(HS, e_g^2 t_{2g}^4, S = 2)$ state, stable at high temperature and a diamagnetic low-spin $(LS, e_g^0 t_{2g}^6, S = 0)$ state,

stable at low-temperature thanks to the ligand field energy of the ligands. It is important to mention for the non-specialist readers that the SCO solids switch between a paramagnetic and a diamagnetic state and do not show magnetic ordering. The main reason for the absence of magnetic ordering in the HS phase of SCO solids is the lack of covalent bonding between the metal ions, which are distant by ~1 nm. Only a few experimental data obtained on the bimetallic coordination polymeric compound[21] have shown the existence of long-range magnetic ordering in SCO materials, which has been modeled using three states spin Hamiltonians[22, 23, 24].

Under the effect of external perturbations, such as a variation of temperature [25-30], pressure [31-36], light irradiation [36-43], electric or magnetic field [44-50], or chemical composition [36, 51-53] etc, the SCO solids may switch reversibly between HS and LS configurations leading to first-order or continuous (gradual) transformations. When the switching takes place through a first-order phase transition, this type of property is referred to as "bistability property" from which originates most of the potential applications of these materials. The switching between the HS and LS states is accompanied by a significant volume change ($\sim 3-5\%$) as widely demonstrated by x-rays diffraction on single crystals [54-57]. Imaging spin-transition by optical microscopy conducted first by Jeftic and Hauser in a $[Fe(ptz)_6](BF_4)_2$ (where ptz=1-n-propyltetrazole) large single crystals pointed out the important role of the thermo-chromic character of these materials [58]. Utilizing this property, Chong et al. revealed the existence of mechanical stresses during the spin transition, evidenced during the volume variation of these systems through the generation of inhomogeneous stresses causing irreversible damage to the crystals [58, 59]. Ogawa et al. [60] reported these inhomogeneous features during the photo-excitation of $[Fe(2\text{-pic})_3]Cl_2$.EtOH (pic=2-picolylamine) using a femtosecond (fs) laser pulse. Indeed, the study of the spatiotemporal aspects of the spin transition phenomenon shows that the nucleation and the growth of LS or HS phases proceed via a single domain process, with a well-defined and visible interface, which moves at constant velocity. It is demonstrated that this propagation process [61, 62] is governed by the mechanical stress effects, through the contribution of the elastic interactions, [58, 63] arising from the volume change at the transition. On the other hand, many experimental studies [37, 61-71] conducted on these complexes showed that a rich variety of spin transition behaviors can be generated. Among them, one may quote: (i) the gradual spin-transition, which could be described by a simple Boltzmann distribution of overall energy levels involved in weak cooperativity system [72, 73, 74]; and (ii) sharp first-order transitions with hysteresis transition [75]. The last points concern (iii) incomplete transitions and (iv) two-step or multi-step transitions [76-82]. The latter, take place with the emergence of ordered intermediate phases, which are stabilized leading to the appearance of one or several plateaus in the thermal-dependence of the order parameters, as reported in several experimental studies,[83-86] which demonstrated the existence of self-organization of the spin states in these regions. The spatial organizations of the spin states were found under the form of antiferro-like (checkerboard) structure[87, 88] or may have more complex structures, like ordered alternate HS and LS sheets as in $[Fe(2\text{-pic})_3]Cl_2$.EtOH (pic=2-picolylamine)[83] or modulated HS-LS patterns, where the modulation can be commensurate or incommensurate with the lattice parameter[84, 85, 86] as obtained in the case of Devil's staircase, where

multiple transitions are observed during the thermal transition. It is important to notice that this multiplicity of transitions is often enhanced by the presence of inequivalent iron sites in the system, which then creates artificially additional plateaus.

From the theoretical point of view, the occurrence of multi-step transitions with self-organization of the spin states in the plateau region has been explained first, in elastic models, as due to a spontaneous elastic frustration[89] that appears in the lattice due to the existence of antagonist (or competing) elastic interactions. Other phenomenological approaches based on the use of anisotropic next-nearest neighbour Ising (ANNNI) model have been also developed[90, 91] and allowed to reproduce the double step transitions as well as the existence of spatial striped self-organization of the spin states along with the spin transition mechanism.

Recently, it has been shown that the behaviors of spin-crossover compounds, in solid state, can be obtained by using quite realistic microscopic models [92-100] based on the elastic descriptions taking into account the volume change of the materials at the transition. These models include in fact the coupling between the spin state structure and the lattice degrees of freedom. Some of them are based on vibronic descriptions of the SCO phenomenon[101, 102, 103] while others used spin-phonon models[104]. In these two types of elastic models, the change of the lattice parameter at the transition has been omitted. Other kind of elastic models including volume change at the transition based on several types of potentials have been proposed. In some, anharmonic Lennard-Jones or Morse potentials were implemented[105, 106, 107], while in others mechanoelastic descriptions taking into account for internal pressure effects[108] are developed, as well as harmonic electroelastic models[92, 93] including explicit spin-distortion coupling. In all these models, the spin-crossover molecules are modeled as atoms with two electronic states [87, 93, 100]: a stable LS state at low temperature and a stable HS state at high temperature. In the case of the electro-elastic model, which will be used in the present work, these atoms are interconnected by springs whose elastic constants and equilibrium distances depend on their spin states [87, 93]. This genuine electro-elastic model, considered here in the general case, takes into account the degree of freedom of the spin states and the positions, and leads to short- and long-range effects [93, 109, 110] whose competition produces self-organization of the spin states. Indeed, several models outlined the interplay between the spin-crossover and the lattice properties which deform the lattice. This deformation of the lattice results from the variation of unit cell volume during the HS ↔ LS transition and is attributed to the long-range interactions, and to the non-homogeneous strains [58, 59, 63, 93, 99, 109, 111]. On the other hand, it must be noticed that the resolution of the electro-elastic Hamiltonian, based on the change of position and spin degrees of freedom by Monte Carlo simulations is highly time-consuming. This is due to the stochastic algorithm that imposes for each spin state change to relax mechanically the lattice by slight displacements of nodes irrespective whether this spin flip is accepted or rejected. Therefore, to reduce the execution time of this sequential resolution, we use, in this contribution, a homogeneous electro-elastic model to study the thermodynamic properties of spin-crossover compounds. This model is derived from the genuine electro-elastic Hamiltonian in the general case. For that, we first consider the elastic constants independent of the spin states, then the total elastic energy of the original 2D Hamiltonian is first minimized with respect to the lattice spacing and then re-expressed rigorously into an

effective 2D Ising-like model, accounting for nearest and next-nearest neighbor interactions. The obtained model is solved by Monte Carlo simulations, based on Metropolis transition rates, from which we derive the thermal and spatiotemporal properties of this elastically homogeneous 2D lattice. Although the present Ising-like Hamiltonian, resulting from the general homogeneous elastic model, does not account for the lattice deformation, it is however more realistic than the usual Ising-like model or Drickamer[112] approaches, used to describe the thermal properties of SCO solids, in which the coupling parameters are purely phenomenological and miss the crucial information about their relation with the elastic interactions.

The paper is organized as follows: in Sec. II, we first present the general version of the genuine 2D electro-elastic model for spin-crossover solids by considering the bond length distances and elastic constants depending on the spin states. Then, from this model, we deduce the homogeneous electro-elastic model equivalent to the Ising model combining long-range ferroelastic, and short-range nearest neighbors (nn) and next-nearest neighbors (nnn) antiferroelastic interactions. Finally, we describe the MC procedure and give the parameters used to solve the elastic Hamiltonian. Sec. III is devoted to the presentation and the discussion of the various thermal dependences of HS fractions and spatiotemporal organizations emerging from the simulations. In Sec. IV, we conclude and outline the possible extensions of the present work.

II. ELECTRO-ELASTIC MODELLING

The electro-elastic model describing the spin transition phenomenon considers a 2D square lattice system of $N \times N$ sites depicted in **Fig. 1**, in which each SCO molecule representing a lattice site is associated with a fictitious spin state, $S_i = \pm 1$, where $S_i = +1$ corresponds to HS state and $S_i = -1$ to the LS state. The Ising description in this model ends here since all interactions between the spin states are taken into account through the local variation of the molecular volume accompanying the spin change. Thus, the sites (nearest neighbors and next-nearest neighbors located along diagonals) are linked by harmonic springs [92, 93, 99]. Their associated elastic constants and the equilibrium distances depend on the spin states of the linked sites. The Hamiltonian describing such system in 2D is given by [92],

$$H = \sum_i \frac{(\Delta - k_B T \ln g)}{2} S_i + \frac{A}{2} \sum_{(i,j)} (r_{ij} - R_0(S_i, S_j))^2 + \frac{B}{2} \sum_{(i,k)} (d_{ik} - d_0(S_i, S_k))^2. \quad (1)$$

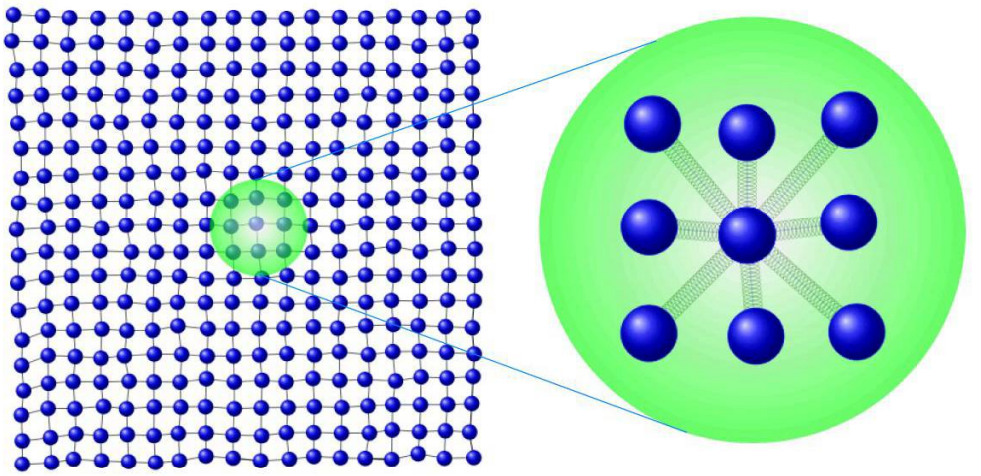

FIG. 1. Left. An example of a non-relaxed spin-crossover lattice in the LS state. Right. Schematic representation of a central site of coordinates (i,j) surrounded by four nearest and next-nearest neighbors. The coordinates of the neighbors (i',j'), are respectively $(i'=i,\ j'=j\pm 1$ and $i'=i\pm 1,\ j'=j)$ for nn and $(i'=i\pm 1,\ j'=j\pm 1)$, for the nnn.

The first term of Hamiltonian (1) is the effective temperature–dependent energy gap between the LS and HS states. It contains the effective ligand field energy contribution, $\Delta_{\text{eff}}=\Delta-k_BT\ln g$, arising from the difference of ligand fields, Δ, in the HS and LS states at $T=0$ K and, the entropic contribution, $k_BT\ln g$, originating from the electronic and vibrational degeneracy ratio, $g=\frac{g_{HS}}{g_{LS}}$, between the HS and LS states. The second and the third terms are the elastic energy contributions between the nearest (nn) and next-nearest neighbors (nnn) of spin-crossover units, respectively.

Let us denote by, R_0^{HH}, R_0^{LL} and R_0^{HL}, the equilibrium distances between nn HS-HS, LS-LS and HS-LS sites, we then have $R_0(+1,+1)=R_0^{HH}$, $R_0(-1,-1)=R_0^{LL}$ and $R_0(+1,-1)=R_0^{HL}$. Due to the Ising character of the fictitious spin describing the electronic state of the SCO molecule, one can easily establish that nn equilibrium bond lengths, $R_0(S_i,S_j)$ appearing in Eq. (1), can be written as a function of the spin states, S_i and S_j under the following form:

$$R_0(S_i,S_j)=\rho_0+\rho_1(S_i+S_j)+\rho_2S_iS_j, \tag{2}$$

where,

$$\rho_0=\frac{\bar{R}+R_0^{HL}}{2},\ \rho_1=\frac{\delta_R}{4},\ \rho_2=\frac{\bar{R}-R_0^{HL}}{2},\ \text{and}\ \delta_R=R_0^{HH}-R_0^{LL}. \tag{3}$$

Here, $\bar{R} = R_0^{HL} = \frac{R_0^{HH}+R_0^{LL}}{2}$ corresponds to the average equilibrium distance between HS and LS phases, and $\delta_R = R_0^{HH} - R_0^{LL}$, is the lattice misfit between the LS and the HS phases.

Due to the 2D character of the lattice, the nnn equilibrium bond length, connecting two spins S_i and S_k along diagonals, is assumed to be equal to, $d_0(S_i, S_k) = \sqrt{2}R_0(S_i, S_k)$.

This model has been resolved in the past for several situations of SCO lattices (1D and 2D) including the case of nanoparticles [113], nanostructures [114]. It also allows us to demonstrate that the multistability observed in a large number of SCO solids may result from the existence of elastic frustrations [93, 96, 98, 115] between the degrees of freedom (distortions, rotations, expansions, and contractions) involved during the spin transition. Although very powerful, the presence of spin and position variables in the model makes generally its treatment quite heavy and requires long-time simulations. Indeed, the resolution of the model includes Monte Carlo simulations on the spin states and extensive molecular dynamics (or MC simulations) for the lattice positions. Therefore, as an alternative approach, we propose to keep the elastic character of the model, which makes its originality and to solve it in the homogeneous case, by adopting a kind of mean-field elastic theory, which then absorbs the lattice variables, which become average quantities depending on the spin states. We checked that within this method, the simulation time is divided by fifty, with high-quality results, as will be demonstrated below.

A. The homogeneous version of the electro-elastic Model and derivation of the Ising-like Hamiltonian

The electro-elastic model described above and used in our previous papers [92, 93] is implemented under its general form. This model shows that the elastic constants, as well as the equilibrium distances between the nearest neighbors (nn) and next-nearest neighbors (nnn) sites, depend on their connected spin states leading to a mutual dependence between distances, elastic constants and spin states. This character highlights the complex interplay between a local field-like contribution, local short-range interactions and a complex long-range elastic contribution, whose sign depends on several parameters. On the other hand, the MC simulations used to study this model are conducted on the spin states and positions. In the way to simplify the study of such 2D square lattice system where the degree of freedom of spins and positions are both taken into account, we use a homogeneous electro-elastic model, which we describe in the following manner.

First, we adopt the situation of a lattice with a homogeneous lattice bond length x between nn and $x\sqrt{2}$ between nnn. The Hamiltonian (1) becomes,

$$H = \sum_i \frac{(\Delta - k_B T \ln g)}{2} S_i + \frac{\mathrm{A}}{2} \sum_{(\mathrm{i,j})} (x - R_0(S_i, S_j))^2 + \frac{\mathrm{B}}{2} \sum_{(\mathrm{i,k})} (x\sqrt{2} - \sqrt{2}R_0(S_i, S_k))^2. \quad (4)$$

The idea here is to minimize first the total energy with respect to variable x in order to reach the mechanical equilibrium. This is done by solving the equation: $\frac{\partial H}{\partial x} = 0$, which leads to the following expression of the relaxed bond length distance,

$$x_{relax} = \frac{A\sum_{ij}^{nn} R_0(S_i, S_j) + 2B\sum_{ik}^{nnn} R_0(S_i, S_k)}{AN_{nn} + 2BN_{nnn}}, \tag{5}$$

where, $N_{nn} = 2N(N-1)$ and $N_{nnn} = 2(N-1)^2$ are the nn and nnn number lattice of bonds, respectively.

By replacing $R_0(S_i, S_j)$ with its expression, given in (2), and considering the case of a large system, which gives $N_{nn} \sim N_{nnn} \sim 2N^2$, the expression of the homogeneous bond length in the minimum elastic energy, becomes after some rearrangements,

$$x_{relax} = \rho_0 + 2m\rho_1 + \rho_2 \frac{Ap + 2Bq}{A + 2B}, \tag{6}$$

Where, $m = < S_i >$ is the average spin value which connects to the HS fraction, n_{HS}, through $n_{HS} = \frac{1+m}{2}$, and $p = < S_i S_j >$ and $q = < S_i S_k >$ are the average nn and nnn spin-spin correlations, respectively. It is important to notice that the dependence of the mechanically relaxed homogeneous bond length on average spin quantities will naturally introduce infinite long-range interaction inside the lattice. This clearly establishes the origin of the long-range nature of the elastic interactions in SCO models, and validates the use of mean-field approaches in describing SCO materials.

Inserting the expression x_{relax} instead of x in (1) and rearranging all terms, we find after some simple algebra, that Hamiltonian (1) can be mapped under the form of an Ising-like Hamiltonian including short- and long-range interactions of elastic nature, whose expression is,

$$H_{relax} = h\sum_i S_i + J_{nn}\sum_{(i,j)}^{nn} S_i S_j + J_{nnn}\sum_{(i,k)}^{nnn} S_i S_k + E_0, \tag{7}$$

where, h, J_{nn} and J_{nnn} are field-like, nn interactions and nnn (along diagonals) interaction terms, whose analytic expressions as a function of the elastic constants, average magnetization and correlations are,

$$h = \frac{(\Delta - k_B T \ln g)}{2} - 4m\rho_1^2(A + 2B) - 2\rho_1\rho_2(Ap + 2Bq) - 2\rho_1\rho_2(A + 2B), \tag{8a}$$

$$J_{nn} = A\left(\rho_1^2 - 2m\rho_1\rho_2 - \rho_2^2\frac{Ap + 2Bq}{A + 2B}\right), \tag{8b}$$

$$J_{nnn} = 2B\left(\rho_1^2 - 2m\rho_1\rho_2 - \rho_2^2\frac{Ap + 2Bq}{A + 2B}\right). \tag{8c}$$

The temperature-dependent energy, E_0, whose expression is, $E_0 = \left(\frac{A}{2}N_{nn} + BN_{nnn}\right)\left[\left(2m\rho_1 + \rho_2\frac{Ap+2Bq}{A+2B}\right)^2 + 2\rho_1^2 + \rho_2^2\right]$, identified as the cohesion energy, doesn't affect the thermodynamic properties of the SCO system, and so it will be omitted in the next developments.

Compared with the usual Ising-like model, Hamiltonian (7) contains true elastic contributions which impact the interaction parameters as well as the effective ligand field, h. The present homogeneous Ising-like Hamiltonian depends on lattice parameters, ρ_1, ρ_2, A, B, as well as on the electronic order parameters, m, p, q which express the macroscopic spin state configuration of the system. This way, the lattice variables have been integrated out, which considerably simplifies the resolution and the treatment of the Hamiltonian.

Another interesting aspect of the model relates to the sign of the interaction parameters. Indeed, depending on the model parameters, the nn and nnn interactions may be positive or negative, which competes with the ferroelastic long-range interactions emerging from the effective field [Eq. (8a)]. On one hand, the homogeneous model is given in Eq. (7), highlights, the link existing between spin states, and distances, indicates that the variation of distances affects the electronic spin states. While, on the other hand, the elastic constants being independent on the spin states any variation to them does not induce any change on the electronic spin states per site but affects the rigidity of the system. Otherwise, the change of distances and elastic constants results in a competition between the ferroelastic long-range field-like and antiferroelastic short-range interactions.

It is worth mentioning that the structure of Hamiltonian (7) recalls that of the well-known ANNNI model[116, 117, 118] since it includes short-range antiferro-like interactions competing with long-range ferro-like interactions. ANNNI model whose complex phase diagram shows many bifurcations is widely used to describe frustration and spin patterning, including spatially-modulated structures. Compared to the present Hamiltonian (7), the nnn antiferro interactions in ANNNI model are taken along x and y-axis of the crystal lattice. Therefore, they correspond to third 3rd nearest neighbors' sites in the case of Hamiltonian (7), in which the 2nd neighbors are considered along the diagonals. Although, there is a clear difference in the interaction structure between the two models, we do think that their phase diagrams may show strong similarities, as indicated by the form of patterns obtained in the present simulations, due to the presence of similar long-range interactions and short-range antiferro coupling.

B. Monte Carlo technique and model parameter values

The study of the thermodynamic properties of the homogeneous electro-elastic 2D model (7) is performed on the 2D square lattice of size $N \times N = 30 \times 30$, with free boundary conditions. Each site interacts with its nearest and next-nearest neighbors. Initially, we prepare the system in the HS (resp. LS) phase by fixing all the spins to $S_i = +1$ (resp. $S_i = -1$) and all nn lattice distances equal to R_0^{HH} (resp. R_0^{LL}). Monte Carlo simulations based on the Metropolis algorithm are performed to solve the present Hamiltonian. To

determine the thermal properties of the system, we first cool down from 200 to 1 K and then warmed up to 200 K, with 1 K increments. At each temperature, we perform 100000 MCS to reach the equilibrium state and we use 100000 other MCS for the statistics. The used model parameter values are as follows: $\Delta = 450$ K for the ligand field energy, $g = 150$ ($\ln g = 5$) for the degeneracy ratio leading to a transition temperature in case of weak interactions, $T_{eq}^{0} = \frac{\Delta}{k_B \ln g} = 90$ K. The values of the nn equilibrium bond lengths are taken equal to $R_0^{HH} = 1.2$ nm ($R_0^{LL} = 1.0$ nm) between two HS (LS) sites. For the HS−LS configuration, we chose $R_0^{HL} = \bar{R} = \frac{R_0^{HH}+R_0^{LL}}{2} = 1.1$ nm which cancels the parameter ρ_2 [see Eq. (3)], thus simplifying considerably the expressions of h, J_{nn} and J_{nnn}. Moreover, the nnn equilibrium distances are simply obtained by multiplying those of nn by the factor $\sqrt{2}$.

III. RESULTS AND DISCUSSIONS

To give an overview of the possibilities offered by this model, we investigate the thermal properties of the HS fraction and the spin-spin correlations with an emphasis on providing the important role of the elastic constants A and B and their natural competing character on the emergence of all types of SCO behaviors, observed experimentally: gradual, first-order, incomplete, two-step and multi-step thermal transitions. The last five-cases originate from the existence of elastic frustration in the lattice and are often accompanied by the emergence of complex spin structures and self-organization along with the thermally-induced spin transition.

A. Isomorphism with the frustrated Ising-like model

First, we analyze the Hamiltonian structure in the case where $R_0^{HL} = \frac{R_0^{HH}+R_0^{LL}}{2}$. As explained above, we then have systematically $\rho_2 = 0$; the relaxed lattice distance becomes $x_{relax} = \rho_0 + 2m\frac{\delta_R}{4}$ and the Hamiltonian writes,

$$H = \left[\Delta_{eff} - 4m\left(\frac{\delta_R}{4}\right)^2 (A+2B)\right]\sum_i S_i + \left(\frac{\delta_R}{4}\right)^2 \left(A\sum_{(i,j)}^{nn} S_iS_j + 2B\sum_{(i,k)}^{nnn} S_iS_k\right). \quad (9)$$

Eq. (9) shows that the effective ligand field energy, $\Delta_{eff} = \frac{1}{2}(\Delta - k_B T \ln g)$, is renormalized by the ferroelastic long-range (mean-field) contribution, $-\frac{1}{4}(A+2B)\,\delta_R^2\, m$. In contrast, the short-range interaction terms, $J_{nn} = A\left(\frac{\delta_R}{4}\right)^2 \sum_{(i,j)}^{nn} S_iS_j$ and $J_{nnn} = 2B\left(\frac{\delta_R}{4}\right)^2 \sum_{(i,k)}^{nnn} S_iS_k$ bring two respective short-range antiferroelastic interactions, $A\left(\frac{\delta_R}{4}\right)^2$ and $2B\left(\frac{\delta_R}{4}\right)^2$ along nn and nnn diagonal directions. The coexistence of nn and nnn antiferro interactions already causes the frustration of the 2D system. This frustration is enhanced by the third long-range contribution, which will generate complex spin state structures. It is important to recall once again that the interaction parameters J_{nn} and J_{nnn} should not be

confused with the exchange coupling interactions of the usual Ising model, since there is no magnetic interaction in this model and in SCO, in general. Although the final form of the Hamiltonian is similar to that of an Ising model, the origin of the interaction parameters is purely elastic in the present model.

In the following, we analyze these frustration effects for different values of the elastic constants A, B through the study of the thermal dependence of the HS fraction, n_{HS}, and spatial self-organization of the spin states along with the thermal spin transition.

B. The case of gradual transition for B<<A

For the small values of B compared to A ($A = 10000\ \mathrm{K} \times \mathrm{nm}^{-2}$, $B = 100\ \mathrm{K} \times \mathrm{nm}^{-2}$), the thermal transition of the HS fraction proceeds via a gradual spin transition between the HS and LS states, as shown in **Figs. 2(a)** and **(2b)** which summarize the thermal evolution of the HS fraction, $n_{HS} = \frac{1+m}{2}$, and the average of nn, $p =< S_i S_j >$, and nnn, $q =< S_i S_k >$, spin-spin correlation, respectively. The transition temperature, is obtained for $n_{HS} = 1/2$ or for the minimum of the quantities $p(T)$ or $q(T)$ which take their maximum values in the LS and HS phases, is indeed around 90 K, as predicted analytically. The selected snapshots, of **Fig. 2(c)**, on cooling, at $T = 118\ \mathrm{K}, 90\ \mathrm{K}$ and $71\ \mathrm{K}$ show that HS ↔ LS transformation occurs through the nucleation and growth of multidroplets forming ramified structures without any clear organization of the spin states. This is due to the weak elastic coupling between the spin states, compared to the effective ligand field energy which stabilizes the LS (HS) phase at low (high) temperature. In agreement with this view of the disordered state in the middle of the transition, the nn correlation function peaks around the transition temperature [**Fig. 2(b)**].

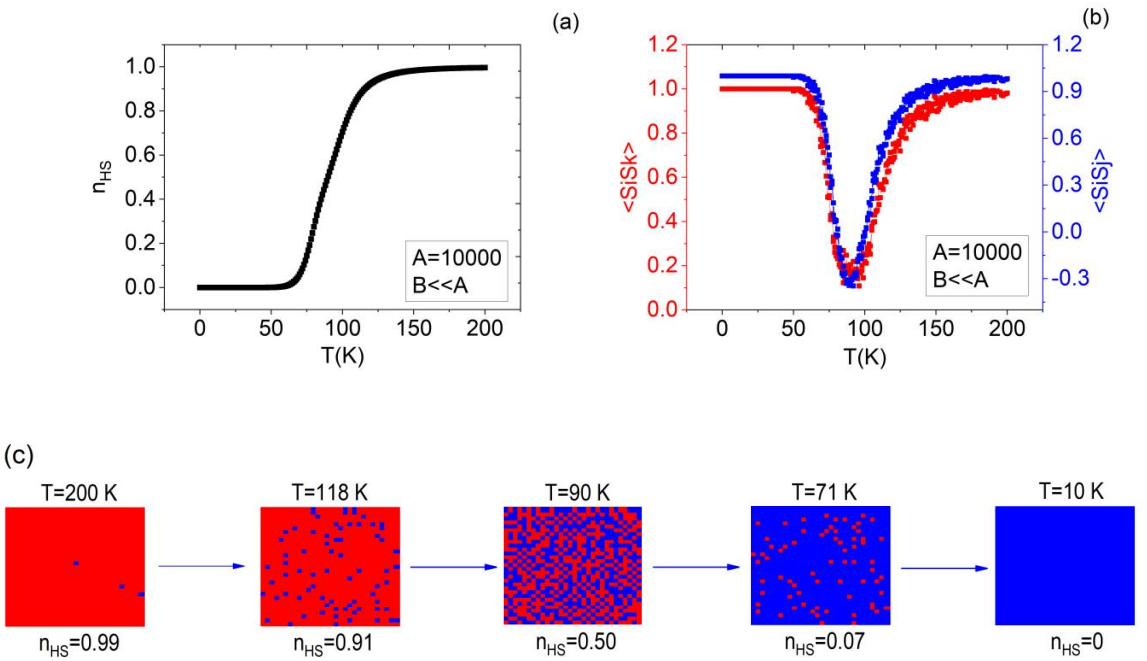

FIG. 2. Thermal-dependence of the (a) HS fraction, n_{HS} and (b) average nn, $< S_i S_j >$ (blue curve) and nnn, $< S_i S_k >$ (red curve), spin-spin correlations showing a gradual spin transition. (c) Snapshots of the ramified spatial organization of the spin states along the thermal transition of this weakly cooperative system. Red (blue) squares represent HS (LS) species.

C. The case of two-steps transition and self-organization of the spin states when B<<A

When increasing the value of the elastic constant A from $A = 10000\ \mathrm{K} \times \mathrm{nm}^{-2}$ while maintaining the nnn elastic constant B negligible, we enhance the anisotropy of elastic constants along x and y directions and the diagonal one. Thus for $A = 20000\ \mathrm{K} \times \mathrm{nm}^{-2}$, the system undergoes a two-step spin transition, characterized by the presence of a very thin thermal hysteresis for the first transition around 72 K, and followed with a continuous (gradual) transition at 115 K, as depicted in **Fig. 3(a1)**. Between these two transition temperatures, a clear plateau where the HS fraction is almost constant ($n_{HS} \sim 0.5$) takes place. The average nn spin-spin correlation, $< S_i S_j >$, depicted in **Fig. 3(b1)**, reaches the value -1 in the plateau region, while the nnn spin-spin correlation, $< S_i S_k >$ tends to $+1$ with fluctuations and clear peaks around the transition temperatures. As a result, an ordering of the spin states in an antiferromagnetic-like feature is observed in **Fig. 3(c1)** at $T = 90$ K. For $A = 30000\ \mathrm{K} \times \mathrm{nm}^{-2}$, the plateau widens and separates a large hysteretic first-order spin transition at low temperature ($T_{eq} = 59$ K) and a gradual one at a higher temperature ($T_{eq} = 115$ K)[see **Fig. 3(a2)** and the related **Figs. 3(b2)** and **3(c2)**]. Increasing more the elastic interaction to $A = 40000\ \mathrm{K} \times \mathrm{nm}^{-2}$, results in a larger intermediate plateau at $n_{HS} = 0.5$ as depicted in **Fig. 3(a3)** [$< S_i S_j >= -1$ and $< S_i S_k >= +1$ in **Fig. 3(b3)**] where the HS and LS species are organized in a checkerboard fashion [see snapshots in **Fig. 3(c3)**], revealing a perfect spatial organization of the spin states in the plateau region. In addition, the two transitions taking place at 48 K and 126 K are now of first-order. The existence of this structure is in direct line with the presence of an antiferroelastic interaction along the x- and y-directions, due to the short-range antiferroelastic interactions $[A\left(\frac{\delta_R}{4}\right)^2 \sum S_i S_j]$ emerging from the exchange contribution of the Ising Hamiltonian, given in Eq. (9). The existence of the plateau is then the result of the competition of this term with the long-range ferroelastic contribution $[-4m\left(\frac{\delta_R}{4}\right)^2 \sum S_i]$ acting in the effective ligand field.

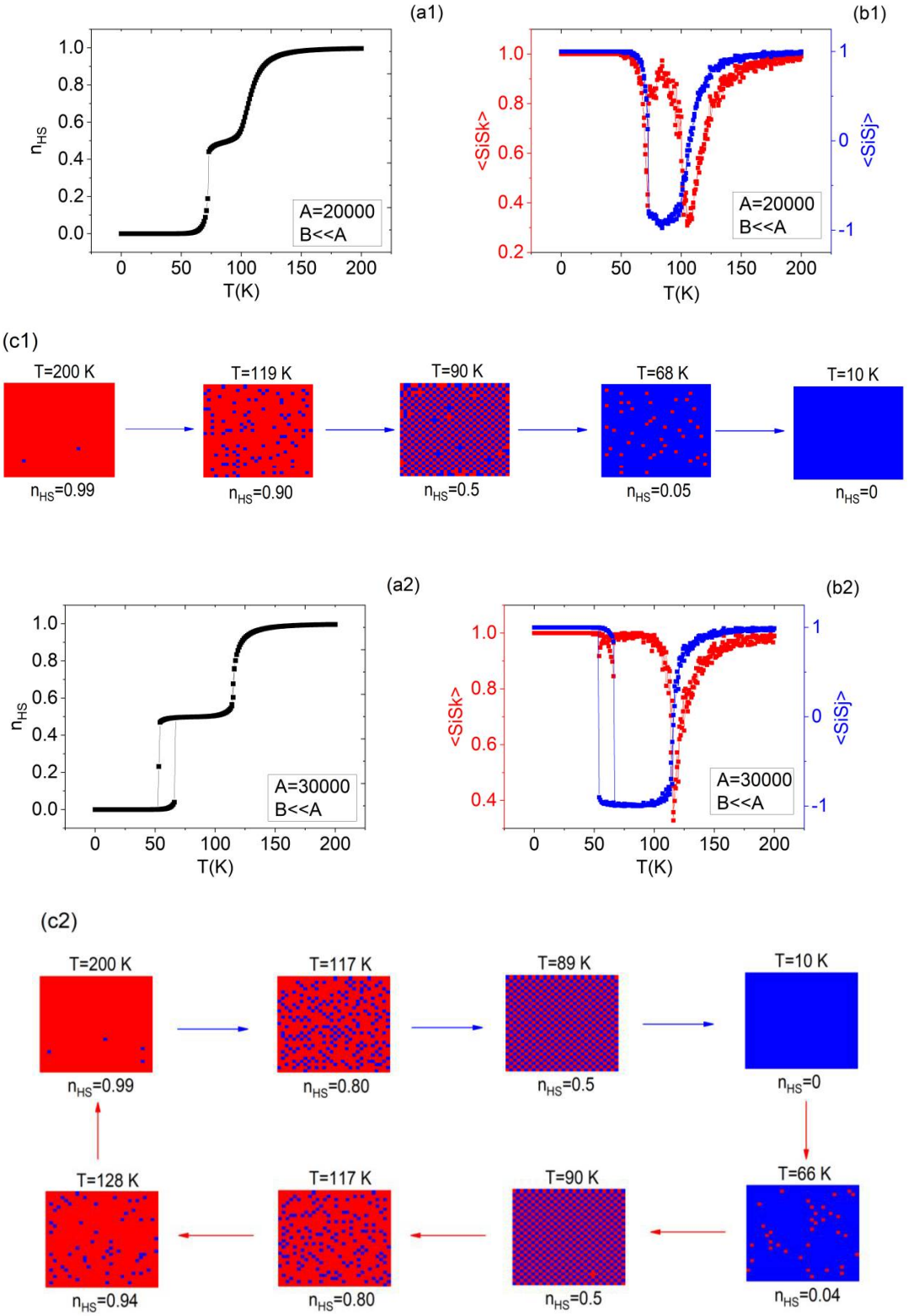

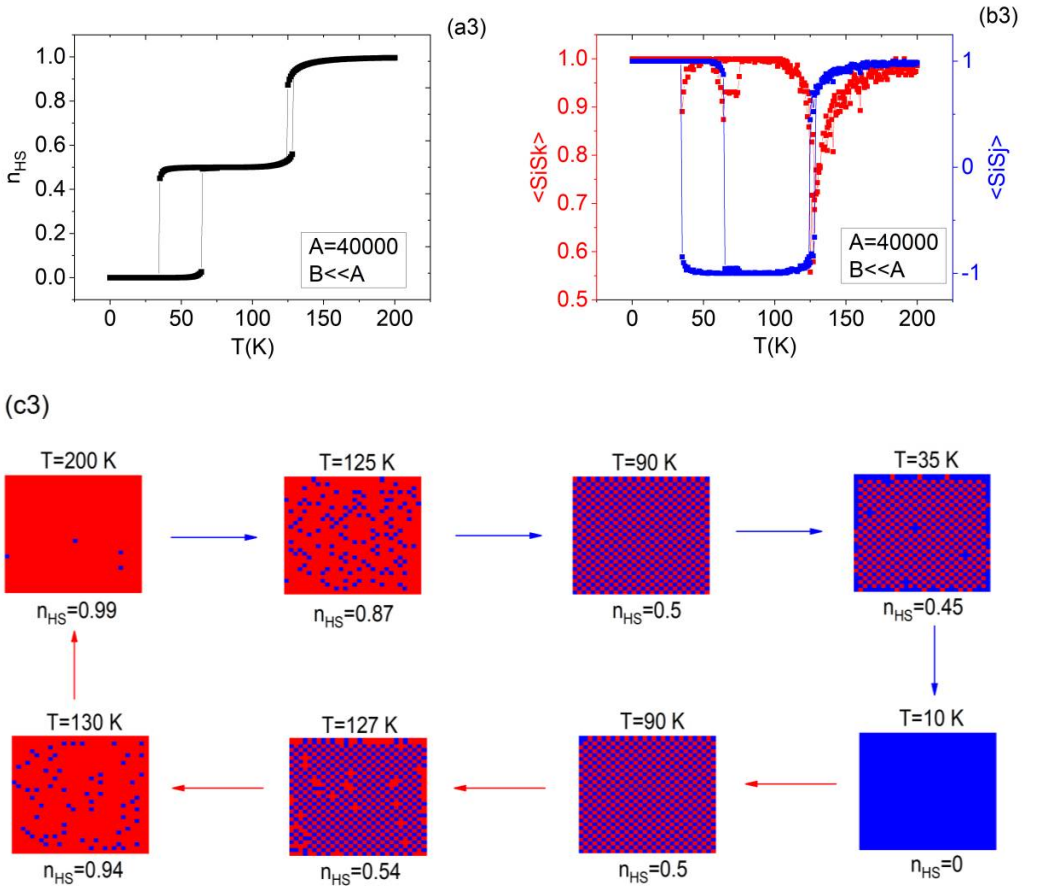

FIG. 3. Thermal-dependence of the (a1-a3) HS fraction, n_{HS} and (b1-b3) average nn, $< S_i S_j >$ (blue curve) and nnn, $< S_i S_k >$ (red curve), spin-spin correlations, for different values of the nn elastic constant, A, showing the presence of two-step transitions with a spatial antiferromagnetic-like organization (c1-c3) of the spin states at $n_{HS} = 0.5$, where HS (red squares) and LS (blue squares) sites alternate along x- and y-directions. Remark the increase of the plateau width, and the change of the nature of the transitions from continuous to first-order with increasing the nn elastic constant, A value.

It is interesting to analyze the occurrence of the perfect antiferro-elastic ordering of the HS and LS sites in the intermediate plateau region of **Fig. 3(a3)** for $A = 40000\ \mathrm{K} \times \mathrm{nm}^{-2}$ and $B = 100\ \mathrm{K} \times \mathrm{nm}^{-2}$, using similar techniques as those of antiferromagnetism. Thus, we define two sublattices, A and B, in such a way that each site A (resp. B) is surrounded by sites B (resp. A) leading to a checkerboard structure, for which we monitor, the thermal dependencies of their associated HS fractions, denoted $n_{HS}^{A} = \frac{1+<\sigma_A>}{2}$ and $n_{HS}^{B} = \frac{1+<\sigma_B>}{2}$. The thermal dependencies of $n_{HS}^{A}(T)$ and $n_{HS}^{B}(T)$ are presented in **Figs. 4(a)** and **4(b)**. First of all, we see that in the full LS and HS states, the sites A and B are equivalent and so we have, $n_{HS}^{A} = n_{HS}^{B}$. In contrast, in the plateau region a clear symmetry breaking occurs during both heating and cooling processes. Thus, for example, on cooling [**Fig. (4a)**], the HS fractions of A and B sublattices are equal in the interval

$200 - 126$ K and then a bifurcation takes place below 126 K, where the A sublattice makes a phase transition from $n_{HS}^{A} = 1$ (HS) to $n_{HS}^{A} = 0$ (LS) while B sublattice remains in HS and keeps the value $n_{HS}^{B} = 1$ until $T = 34$ K, where it converts to LS. Below 34 K, the two sublattices become again equivalent. A similar scenario occurs during heating [**Fig. (4b)**], where the symmetry breaking between the two sublattices takes place at 73 K.

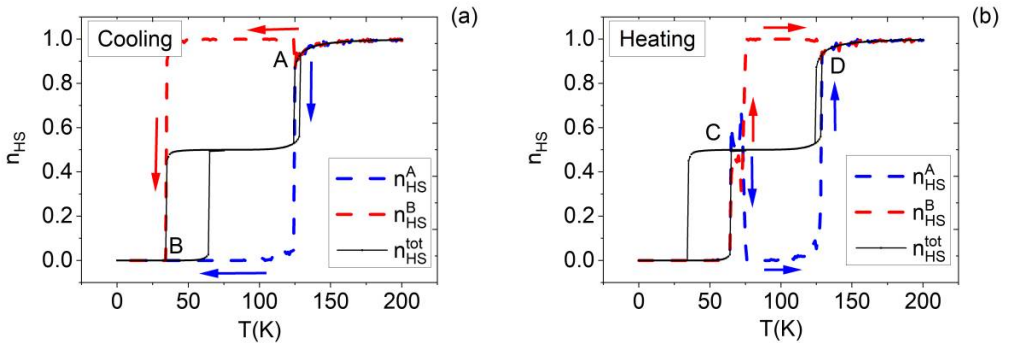

FIG. 4. Thermal-dependence of HS fractions, n_{HS}^{A} (blue dashed curve) and n_{HS}^{B} (red dashed curve) of the two sublattices, A and B, in the coexistence region of the plateau, on cooling (a) and on heating (b) and the total HS fraction, n_{HS}^{tot} (black curve), for $A = 40000\ \mathrm{K} \times \mathrm{nm}^{-2}$ and $B = 100\ \mathrm{K} \times \mathrm{nm}^{-2}$. The black continuous line is the total HS fraction. The bifurcations of the sublattices order parameters, n_{HS}^{A} and n_{HS}^{B} at points A and B (resp. C and D) on cooling (heating) announces the presence of a symmetry breaking between A and B sublattices.

D. The case of incomplete spin transition and hidden stable LS state when $B << A$

Considering the values of the elastic constant A beyond $50000\ \mathrm{K} \times \mathrm{nm}^{-2}$, and proceeding as in experiments by cooling the system from the high-temperature phase (HS) to the low-temperature phase (LS) and then heating again, we find that the lowest transition temperature, T_1^-, on cooling reaches zero [**Fig. 5(a)**], which means that the metastable intermediate state survives until 0 kelvin. The stabilization of this intermediate antiferromagnetic-like state [$n_{HS} = 0.5, < S_i S_j > = -1$ and $< S_i S_k > = +1$ in **Fig. 5(b)**] at low temperature is mainly due to the decrease of thermal fluctuations on cooling. On the other hand, the increase of the elastic constant, A, enhances the energy barrier between the HS−LS and the fundamental LS states, which in turn enhances the lifetime of the metastable intermediate state. So, strong elastic constants stabilize the spin and lattice structures by increasing the elastic energy of the intermediate HS−LS state, which then precludes its transition towards the LS state. **Figure 5(a)** shows clearly that the HS fraction switches in a first-order fashion between the HS state and an intermediate ordered HS−LS state at low-temperature [see snapshots in **Fig. 5(c)**]. The metastable nature of this state is evidenced in **Fig. 6(a)** and **Fig. 6(b)**, where we repeated the thermal cycling by starting the Monte Carlo simulations from the LS state, for $A = 90000\ \mathrm{K} \times \mathrm{nm}^{-2}$. There, a clear hidden LS state appeared, which becomes stable until ~ 60 K, a

temperature at which the system switches from the LS state to the intermediate HS−LS state, leading to a double step transition. The snapshots of the spatial organization of the spin states indicate a perfect antiferromagnetic-like organization of the SCO species, as shown on heating at 100 K in **Fig. 6(c)**. In addition, it is found that the width of the plateau region (**Fig. 7**) increases linearly with the elastic constant in agreement with the increase of the transition temperature and the thermal hysteresis width of the high-temperature thermal hysteresis. It is worth mentioning that this situation of existence of hidden spin states is in excellent agreement with experimental results [88, 119-121], where usually the LS state is reached by applying pressure from the intermediate state [122] or by light through reverse-LIESST process usually using a red light [120, 121, 123].

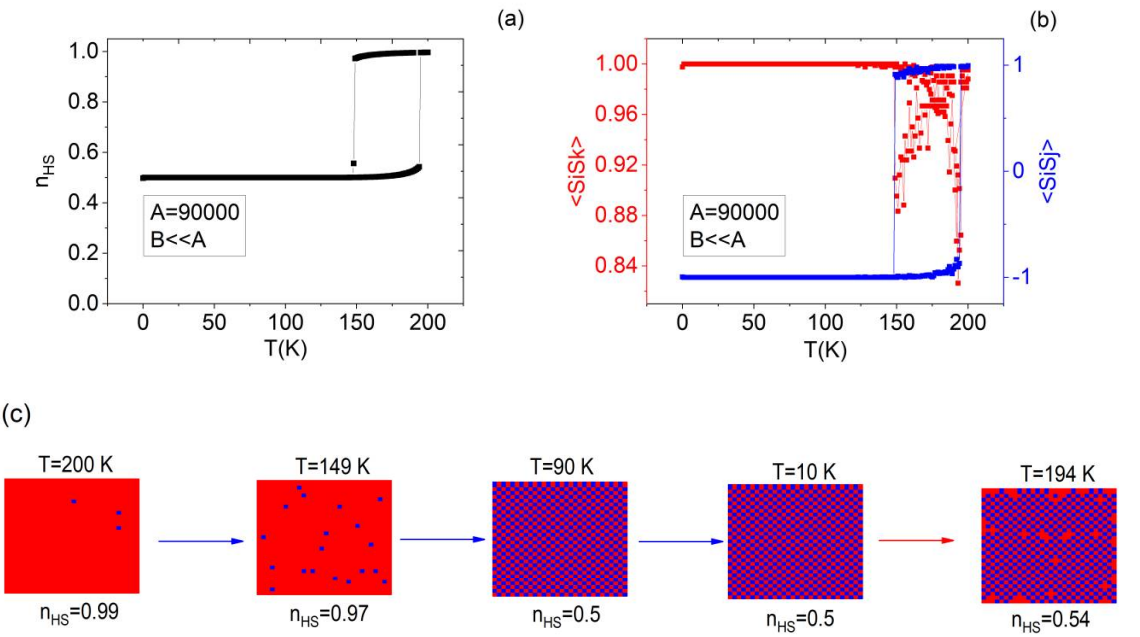

FIG. 5. Thermal-dependence of the (a) HS fraction, n_{HS} and (b) average nn, $< S_i S_j >$ (blue curve) and nnn, $< S_i S_k >$ (red curve), spin-spin correlations, for $A = 9\ 10^4$ K × nm^{-2}, showing an incomplete spin transition at very low temperature with an antiferro metastable intermediate plateau at $n_{HS} = 0.5$. (c) Selected snapshots showing the spatial organization of the HS (red squares) and LS (blue squares) sites, associated with thermal transition curves.

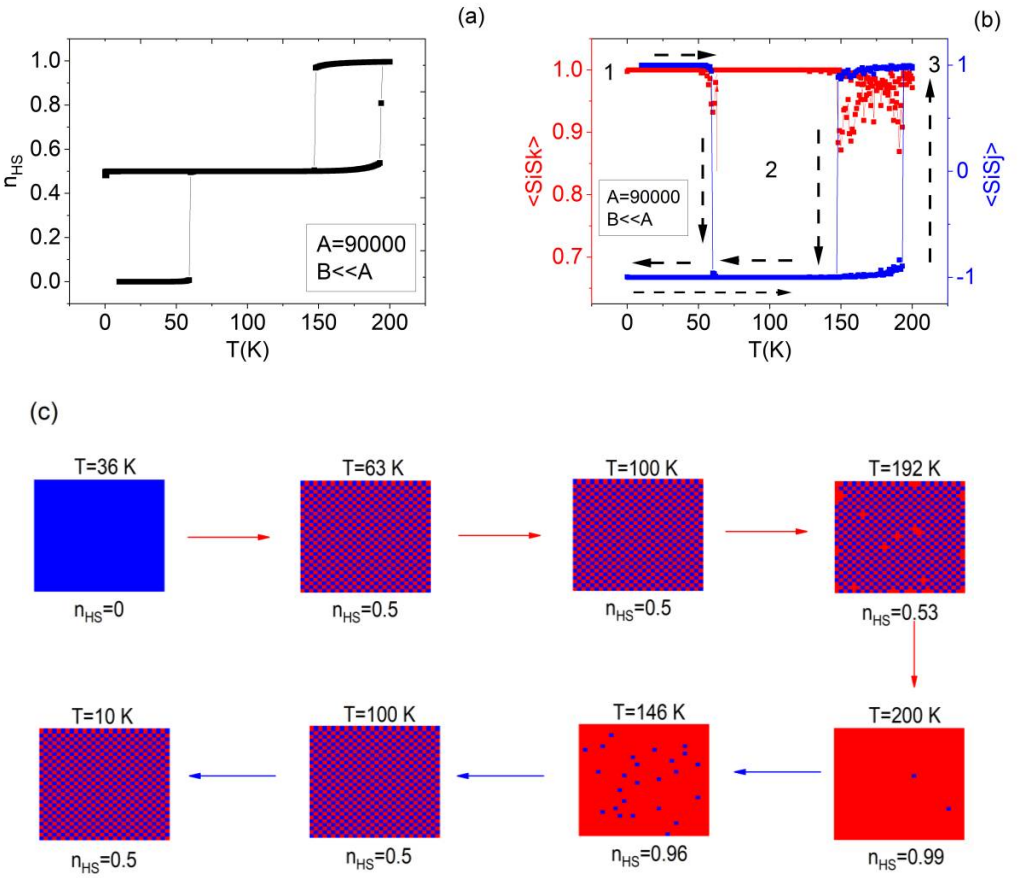

FIG. 6. Thermal-dependence of the (a) HS fraction, n_{HS} and (b) average nn, $< S_i S_j >$ (blue curve) and nnn, $< S_i S_k >$ (red curve), spin-spin correlations, for $A = 9\ 10^4$ K × nm^{-2} showing double step transition with a hidden stable LS state. Remark in (a) that the LS state remains stable until $T \sim 60$ K and then switches to the intermediate plateau. (c) Selected snapshots highlighting the spatio-temporal behaviour of the HS and LS sites, associated with thermal transition curves and showing self-organization of the spin states. Blue and red squares correspond to LS and HS sites, respectively.

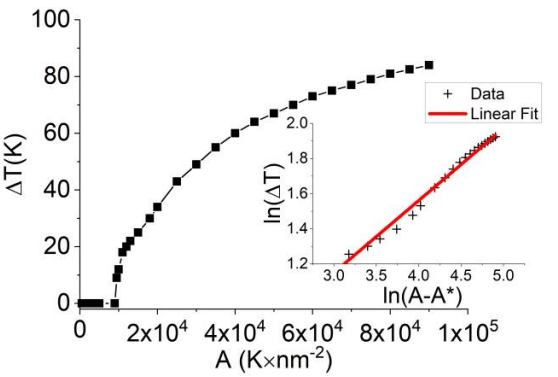

FIG. 7. Nearest neighbours elastic constant, A, dependence of the thermal width, ΔT, of the HS−LS plateau showing a typical second-order phase transition behaviour. Inset: quasi-linear increase of the plateau's width with the elastic interaction following the law of $\Delta T = (A - A^*)^{\alpha}$, with $\alpha = 0.4106$.

Figure 7 depicts the dependence of the thermal width of the plateau, (ΔT), as a function of the nn elastic constant, A. Here, it is revealed that $\ln(\Delta T) = \alpha \ln(A - A^*)$, with $\alpha = 0.4106$ (see inset of **Fig. 7**, indicating that during the thermal evolution, the plateau width follows a power law $\Delta T = (A - A^*)^{\alpha}$. The shape of the curve $\Delta T(A)$ and the value of the exponent, α, close to 0.5, suggest the existence of a second-order critical regime in the behavior of the thermal width of the plateau.

E. Phase diagram

Figure 8 displays the system's phase diagram, in the space of coordinates temperature versus nn elastic constant, A, for a fixed elastic constant $B = 100\ 10^4\ \mathrm{K \times nm^{-2}}$, where we plot the transition temperature, whatever this transition is gradual or first-order, as function of the elastic constant. We notice the existence of several regions. The first region is obtained for, $A < 1.3\ 10^4\ \mathrm{K \times nm^{-2}}$, corresponds to simple gradual transitions between the LS and HS states, in which the transition temperature is independent of the used elastic constant. For $A = 1.3\ 10^4\ \mathrm{K \times nm^{-2}}$, a bifurcation point $\mathrm{P_1}$ $(90, 1.3\ 10^4)$ appears, and two continuous (gradual) transitions lines (T_2 and T_1) take place. The lower (resp. upper) one subsists until the critical point $\mathrm{P_2}$ (70, $22.0\ 10^4$) [resp. $\mathrm{P_3}$ (130, $4.0\ 10^4$)], from which it transforms to the first-order transition (dashed lines) with transition temperatures T_1^+ and T_1^- (T_2^+ and T_2^-). On increasing A, T_2^+ and T_2^- increase as well as their difference $\Delta T_2 = T_2^+ - T_2^-$, which corresponds to the width of the corresponding thermal hysteresis. In contrast, on increasing, A, T_1^+ first decreases and then saturates, while T_1^- tend downwards and vanishes at point $\mathrm{P_4}$ (0, $5.5\ 10^4$). Therefore, to partially summarize, this region, $1.3\ 10^4 < A < 5.5\ 10^4$ corresponds to the plateau region where two spin-crossover transitions are obtained. Both transitions are gradual if, $1.3\ 10^4 < A < 22.0\ 10^4$, then the lower becomes first-order and the upper remains gradual in the region $22.0\ 10^4 < A < 4.0\ 10^4$ finally, both are first-order in the region $4.0\ 10^4 < A < 5.5\ 10^4$. In all these regions, the obtained two-step transitions are complete and antiferro-like ordering do emerge in the simulations. In the region beyond, $A_c = 5.5\ 10^4\ \mathrm{Knm^{-2}}$, starting the MC simulations from the HS state will lead the system to stay in the intermediate state (**Fig. 5**) at low-temperature because the lowest branch of the thermal hysteresis has vanished. On the other hand, the LS state becomes a hidden state, which can be reached from the plateau, using red light through reverse Light-Induced Excited Spin state trapping (LIESST) as in Ref. 88, 120, 121, 123 or by applying pressure from the intermediate state Ref. 122 forcing the system to switch to LS.

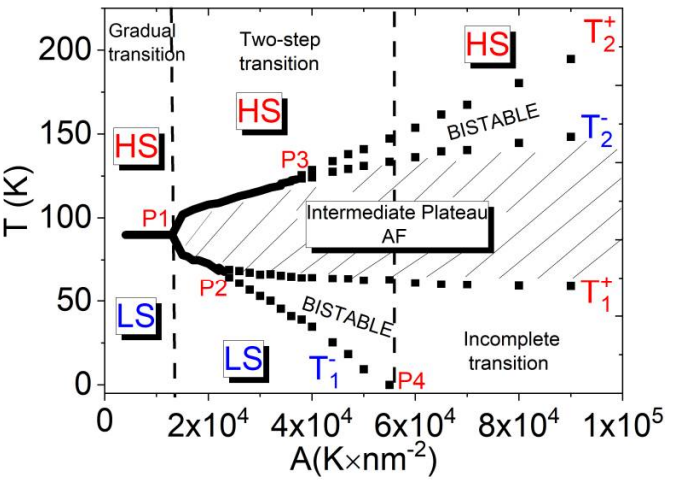

FIG. 8. Phase diagram temperature versus nn elastic constant, A ($B << A$) showing the existence of several regions with different system's thermodynamic properties. The full lines stand to continuous transitions and the filled square symbols correspond to first-order phase transitions. Five thermodynamic regions are identified according to A parameter values. (i) Below bifurcation point P_1, $A < 1.3\ 10^4$ one continuous transition, (ii) between P_1 and the critical point P_2 ($1.3\ 10^4 < A < 22.0\ 10^4$) two consecutive continuous transitions, (iii) between P_2 and the 2nd critical point P_3 ($22.0\ 10^4 < A < 4.0\ 10^4$) a first-order transition followed with a continuous one, (iv) between points P_3 and P_4 (vanishing of the cooling branch of the lower hysteresis) two consecutive first-order transitions, and (v) beyond P_4 incomplete first-order transition, with quenched intermediate state. The hatched area represents the region of the existence of a plateau with the occurrence of antiferro-like self-organization of the spin states. T_2^+ and T_2^- (resp. T_1^+ and T_1^-) are the transition temperatures delimiting the upper (resp. lower) thermal hysteresis of the system. All parameter values are the same as those of **Figs. 2-6**, except for the elastic constant, A.

F. Frustration along the diagonals (B>>A)

Now, we consider the case, $A \ll B$, where nn elastic constant, A ($A = 100\ \mathrm{K} \times \mathrm{nm}^{-2}$), is very small compared to the nn elastic constant, B. Since the short-range interactions are antiferro-like, the behaviour of the system will depends essentially on the quantity, $2B\left(\frac{\delta_R}{4}\right)^2$, which dominates the short and the long-range contribution part. So compared to the previous case, the long-range ferroelastic interactions are now competing with antiferro- diagonal interactions. Due to this different directional interaction, we expect to observe different type of spatial organization of the spin states in the plateau regions. Indeed, in this particular case, ordered intermediate states, with $n_{HS} = 0.5$, should lead to obtaining longitudinal successions of HS stripes and LS stripes. However, due to the square symmetry of the lattice, this configuration is equivalent to that of horizontal alternation of HS and LS stripes.

G. Two-steps transition and labyrinth formation

Similarly, to the previous case, we start the simulations from the HS state (all spins fixed at $S_i = +1$ and all nn distances are set equal to $R_0^{HH} = 1.2$ nm). The simulations are now performed for different values of, B parameter. The evolution of the thermal dependence of the HS fraction, n_{HS}, and that of the nnn spin-spin correlation, $< S_i S_k >$ (eventually that of the average nn spin-spin, $< S_i S_j >$) as well as the spatial spin state organization are summarized in **Figs. 9(a1)**, **(b1)**, **(c1)** for $B = 10000\ \mathrm{K} \times \mathrm{nm}^{-2}$ and in **Figs. 9(a2)**, **(b2)**, **(c2)** for $B = 20000\ \mathrm{K} \times \mathrm{nm}^{-2}$. Two-step transitions with a plateau at $n_{HS} = 0.5$ are got in both cases.

For $B = 10000\ \mathrm{K} \times \mathrm{nm}^{-2}$ [**Fig. 9(a1)**], a weak plateau separates with two gradual spin transitions at low (73 K) and high temperature (108 K). The corresponding $< S_i S_k >$ curve [**Fig. 9(b1)**] peaks in the plateau region give in the plateau region, almost approaching the value -1, which means that the system -1 presents a high degree of ordering. These results well agree with the snapshots of the system, depicted in **Fig. 9(c1)**, showing that at the first transition from HS to the intermediate state at 90 K, HS and LS states are first organized in the form of horizontal stripes which transforms to labyrinths due to the coexistence of horizontal and vertical ferroelastic 1D HS and LS structures. By increasing B to $20000\ \mathrm{K} \times \mathrm{nm}^{-2}$, the plateau also widens **[Fig. 9(a2)]** and leads to the presence of two "hysteretic" first-order spin transitions at low ($T_{eq} = 49$ K) and high ($T_{eq} = 124$ K) temperatures. There, the thermal behavior of the correlation parameter $< S_i S_k >$ [**Fig. 9(b2)**] is just a mirror of the HS fraction, while the spatial organization of the spin states display a perfect order in the plateau regions ($\sim$90 K). In contrast, on each side, complex structures appear which consist of a mixture of alternate ferro-antiferro ordering and labyrinth configurations, formed by the alternate of HS and LS ferromagnetic-like stripes along the x- or y-directions, and interrupted by antiphase boundaries and some disorder. These phases appear in snapshots of **Fig. 9(c2)** on cooling (resp. heating) at snapshot temperatures $T = 120$ and 50 K (resp. 125 K).

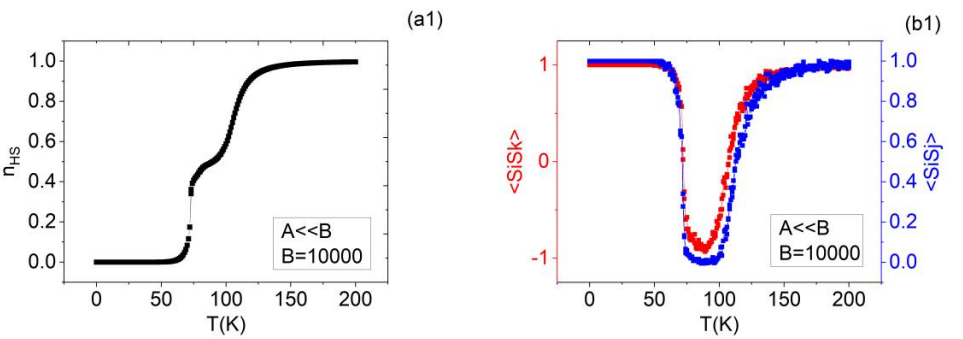

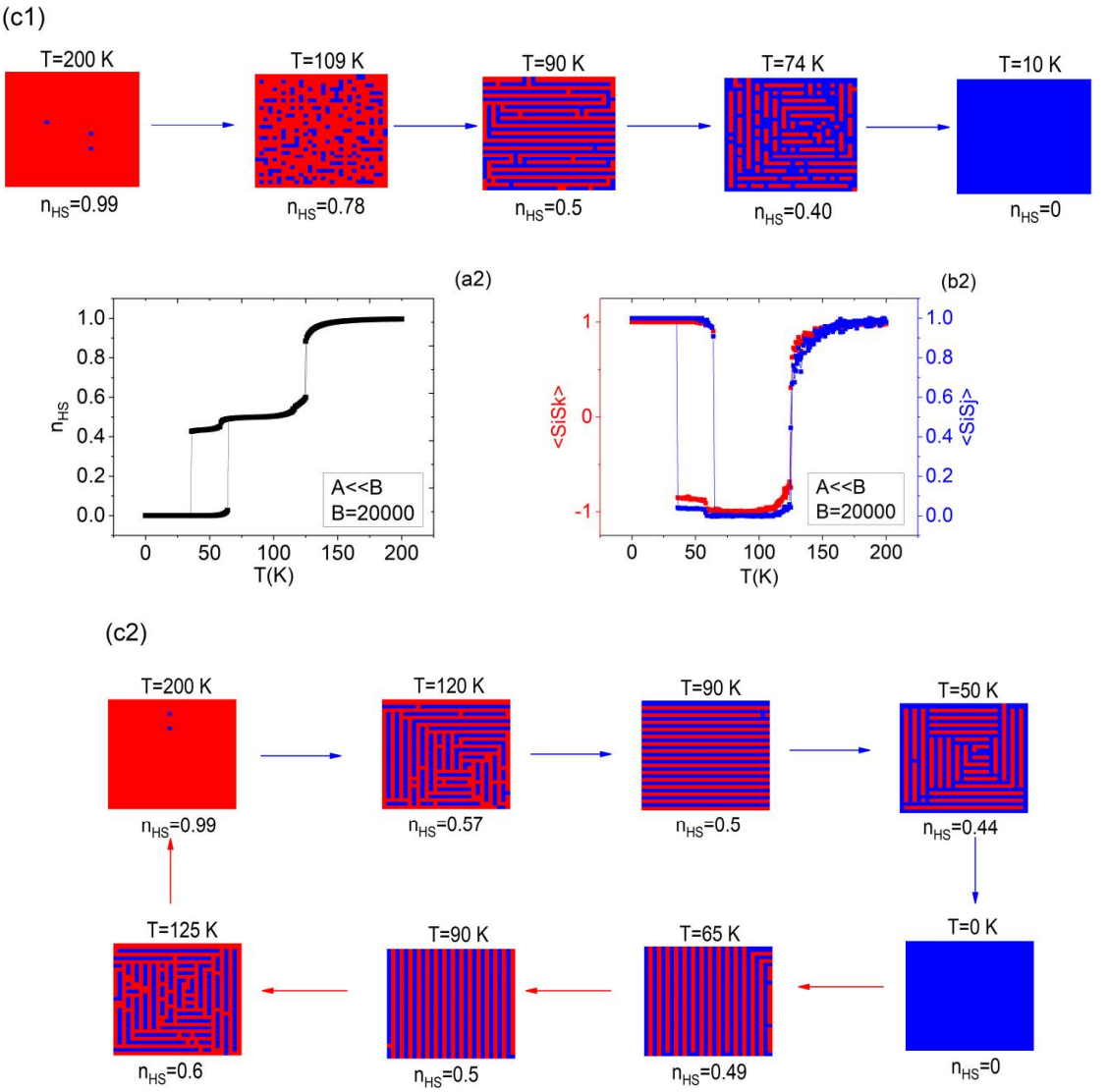

FIG. 9. Thermal-dependence of the (a) HS fraction, n_{HS} and (b) average nn, $< S_i S_j >$ (blue curve) and nnn, $< S_i S_k >$ (red curve), spin-spin correlations, for different values of the nnn elastic constant $B \gg A$, showing two-steps transition with a plateau at $n_{HS} = 0.5$, where the nnn spin-spin correlation, $< S_i S_k >= -1$ indicating an antiferromagnetic-like organization at $T = 90$ K. (c) Selected snapshots of the spatial organization of the HS (red) and LS (blue) sites, associated with thermal transition curves. Remark the macroscopic alternate HS and LS stripes along the x-and y-directions in the plateau regions.

In the same way as beforehand, the increase of the nnn elastic constant B from its previous value, 100 to $B = 3.0\ 10^4$ and $4.0\ 10^4 \mathrm{K} \times \mathrm{nm}^2$, results in the stabilization of the intermediate state until 0 K, leading to incomplete spin transitions, as presented in **Fig. S1** of the supplemental material. Here also, complex structures mixing 1D ferroelastic structures along x- and y- directions are obtained in both cases. On the

other hand, starting the simulations from the LS state also allows demonstrating the presence of a hidden stable LS state whose transition on heating to the intermediate state depends on B parameter. These results are summarized in **Fig. S2** of the supplemental material also demonstrate the appearance of complex structures around the thermal transitions from LS to the intermediate state and from the latter to the stable HS state.

Following the same reasoning as for **Figs. 4(a)** and **4(b)**, we describe the perfect alternate ferroelastic stripes of **Fig. 9(c2)**, obtained for $B = 2.10^4$ K × nm^{-2} and $A = 100$ K × nm^{-2}, we also define two sublattices A and B which consist of horizontal (or vertical) stripes (this configuration is two times degenerate) that we monitor along the cooling and heating branches of the thermal hysteresis. Again, the associated HS fractions of these two sublattices are denoted, n_{HS}^{A} and n_{HS}^{B}, and their thermal evolution are presented in **Figs. 10(a)** and **10(b)** along with that of the total HS fraction, for the cooling and heating regimes respectively, in addition to the total HS fraction of the system, which is given for comparison. Thus on cooling from, $T = 200$ K, the two sublattices remain equivalent until $T = 125$ K, where a symmetry breaking occurs at this temperature for $n_{HS}^{A} = n_{HS}^{B} \sim 0.57$. Interestingly, we remark that until 121 K, the system self-organizes in the form of a ramified HS and LS stripes ordered along x- and y-directions, leading to a labyrinth formation. Below, 121 K, i.e. in the plateau regime, this ramified structure evolves towards a perfectly ordered pattern made of HS stripes ordered along the x-direction, reached around 90 K. Below this temperature, the LS state grows from the surface, as we see at $T = 50$ K for $n_{HS} = 0.44$ on cooling in **Fig. 9(c2)**, and again the ramified (labyrinth) HS-LS structure reappears before disappearing below 33 K. A similar behaviour is also observed during heating where the ordered patterns are now obtained along the y-direction. **Figures 10(a)** and **10(b)** which summarize these behaviours through the thermal dependences of the HS fraction of the two sublattices, $n_{HS}^{A}(T)$ and $n_{HS}^{B}(T)$, shows two bifurcation points during cooling (resp. heating) between 200 K and 1 K located at points E and F (resp. H and G) of coordinates (126 K, 0.94) and (34 K, 0) [resp. (73K, 0.5) and (128 K, 0.93)], confirming the existence of a symmetry breaking between the two sublattices.

The phase diagram corresponding to the present case, $A << B$, is reported in **Fig. S3.** It shows very similar trends with that of **Fig. 8**, with the existence of several regions of B parameter: (i) two consecutive gradual transitions, (ii) a first-order transition followed with a gradual transition and at the end (iii) an incomplete first order transition, with a large plateau.

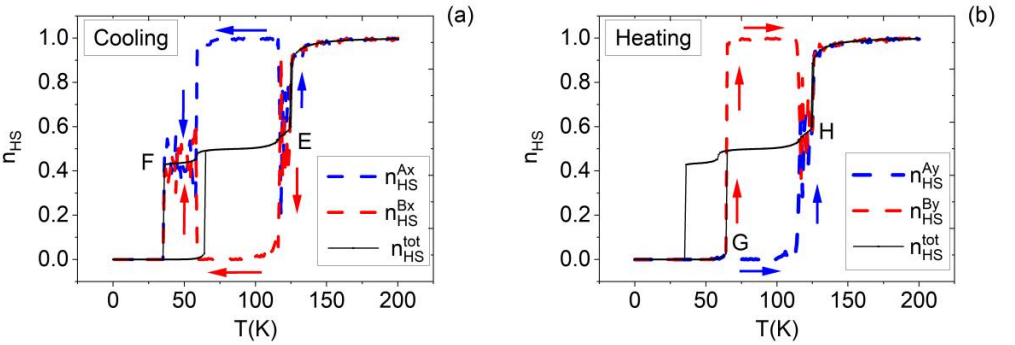

FIG. 10. Thermal-dependence of HS fractions, n_{HS}^{A} (blue dashed curve) and n_{HS}^{B} (red dashed curve) of the two sublattices, A and B, constituted of alternate stripes in the coexistence region of the plateau, during cooling (a) and heating (b) and the total HS fraction, n_{HS}^{tot} (black curve), for $B = 2\ 10^4\ \mathrm{K} \times \mathrm{nm}^{-2}$ and $A = 100\ \mathrm{K} \times \mathrm{nm}^{-2}$. The black continuous line is the total HS fraction. The alternate stripes are along x-direction (y-direction) on cooling (resp. heating) and are characterized by their order parameter $n_{HS}^{A,m}$ and $n_{HS}^{B,m}$ where $m = x,\ y,$ denotes the direction of the stripes. Clear symmetry breaking appear at point E on cooling and point G on heating.

H. Competing short- and long-range interactions: multiple spin transitions

To go further in the analysis of the thermal property investigations of our 2D homogeneous spin-crossover system, we investigate now the case where the short-range nn and nnn antiferroelastic short-range interactions, $A\left(\frac{\delta_R}{4}\right)^2$ and $2B\left(\frac{\delta_R}{4}\right)^2$, have the order of magnitude and competes with the ferroelastic long-range interaction emerging in the ligand-field energy $\left[\frac{1}{2}(\Delta - \mathrm{k_B T \ln g}) - 4m\left(\frac{\delta_R}{4}\right)^2 (A + 2B)\right]$. The existence of the nn and nnn antiferroelastic interactions already cause frustration in the 2D system, as one can easily find since the first one prefers checkerboard structures while the second one stabilizes ferroelastic 1D strings coupled in antiferro-elastic fashion leading to alternate horizontal or longitudinal HS and LS strings. Adding a long-range order to these two contributions adds complexity to the problem. The interplay between the above three contributions gives many types of behaviors which are summarized in the figures below, where the thermal dependence of the HS fraction, n_{HS}, and those of the average nn and nnn spin-spin correlations, $< S_i S_j >$ and $< S_i S_k >$, as well as the spatial organizations of the spin states along the thermal transition branches, are presented. All MC simulations are performed by starting from an initial HS state, where all spins are set equal $+1$ and all distances are set to 1.2 nm.

We started first the simulations with relatively low values of nn and nnn elastic constants, taking $A = 2B = 2\ 10^4\ \mathrm{K} \times \mathrm{nm}^{-2}$, in order to have the same energetic contribution from the two short-range interactions. The results of the temperature-dependence of the HS fraction, n_{HS}, and the average nn and

nnn spin-spin correlations are summarized in **Figs. 11(a) and 11(b)**, which presents a three-step spin transition where all transformations are gradual, with the presence of a clear plateau around $n_{HS} = 0.5$ in the temperature interval of 90-100 K ($< S_iS_k >$ tends to -1 and $< S_iS_j >$ to 0) and another accident on the HS fraction at n_{HS} ~0.2 corresponding to 72 K. The associated snapshots [**Fig. 11(c)**] indicate that in the plateau region at $n_{HS} = 0.5$ (snapshot at $T = 90$ K) the spatial organization of the spin states displays labyrinth formation, which generally expresses dominant nnn interactions stabilized by long-range elastic order. In contrast, for n_{HS} ~0.2 ($T = 72$ K), we see rather a formation of alternate ferro-antiferro-order with the presence of disorder.

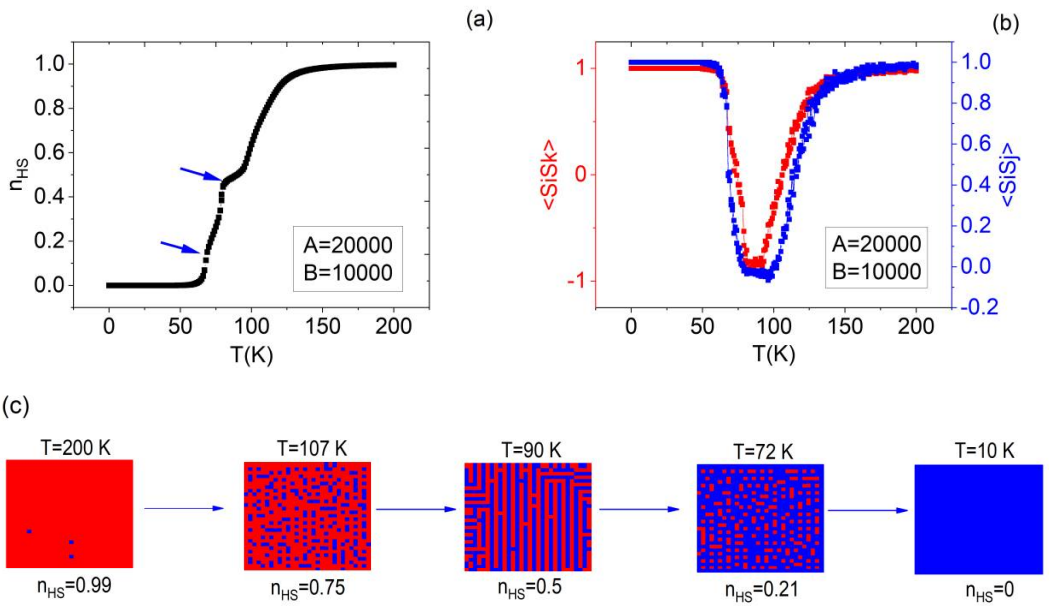

FIG. 11. (a) Thermal-dependence of the HS fraction, n_{HS}, showing a three-step transition with a slight accident around n_{HS}~0.2 and an intermediate plateau at n_{HS}~0.5. (b) Thermal-dependence of the associated average nn, $< S_iS_j >$ (blue curve) and nnn, $< S_iS_k >$ (red curve), spin-spin correlations, (c) snapshots of the spatial organization of the HS and LS sites at selected temperatures along the spin transition. Labyrinth structures are obtained at 90 K, in the plateau region. Elastic constants values are: $A = 2B = 2\ 10^4$ K × nm^{-2}.

Now, we increase the nn and nnn elastic constants ($A = 5\ 10^4$ K × nm^{-2}) while keeping the constraint $A = 2B$, for which, we have $J_{nn} = J_{nnn}$ [Eq. (9)]. The results are summarized in **Fig. 12(a)**. As a consequence, the previous three steps character of **Fig. 11(a)** is enhanced, with larger plateaus, and two of the previous gradual transitions become now first-order with thermal hysteresis. Overall, the LS to HS transformation is accompanied by the presence of three plateaus located at n_{HS}~$\frac{1}{2}$ n_{HS}~$\frac{1}{4}$ and n_{HS}~$\frac{3}{4}$. In these plateaus, the corresponding nn and nnn average spin-spin correlations ($< S_iS_j >$, ($< S_iS_k >$),

represented in **Fig. 12(b),** are respectively equal to $(0,-1)$ for $n_{HS}\sim\frac{1}{2}$, $(0,0)$ for $n_{HS}\sim\frac{1}{4}$ and $(0,0)$ for $n_{HS}\sim\frac{3}{4}$. On heating from LS state, one encounters the first intermediate at $n_{HS}\sim\frac{1}{4}$, which is reminiscent of the last plateau which appeared on the cooling branch in **Fig. 11(a)**. Moreover, the analysis of the spatial distribution of the spin states [**Fig. 12(c)**] shows that during the first transition from HS to the intermediate state ($n_{HS}\sim\frac{3}{4}$), the LS species emerges by forming an antiferromagnetic-like checkerboard structure characterized by the presence of disorder due to thermal fluctuations, i. e. the LS phases appears by forming incomplete strings of antiferromagnetic-like structures coexisting with ferromagnetic-like HS strings distributed along x- and y-directions with the presence of antiphase boundaries. In contrast, in the second plateau region, located at $n_{HS}=0.5$ (see snapshots $T=90$ K), we notice the presence of a highly-ordered spatial self-organization under the form of coexisting HS and LS stripes oriented along the x-direction (resp. along the y-direction) on heating (resp. on cooling). Therefore, on heating, the system stabilizes ferroelastic organization of the spin states along the x-direction and antiferro-elastic one along the y-direction while on cooling it stabilizes ferroelastic organization of the spin states along the y-direction and antiferro-elastic one along the x-direction, even though we did not introduce in the Hamiltonian any anisotropy of interactions. Thus this type of spatial self-organization made of alternate ferroelastic HS/LS strings along x-direction or y-direction is clearly an emerging process at the macroscopic scale, which recalls the dissipative structures observed in Turing patterns [124]. At 10 K, the system reaches the LS state and on heating the first reached plateau at $n_{HS}=0.25$ shows at 61 K a different organization than that at 90 K on cooling. Indeed, here the system self-organizes under alternating along y-direction and along x-direction of ordered LS and HS-LS strings. It is easy to check that this ordered state leads to HS fraction, $n_{HS}=\frac{\frac{N}{2}\times\frac{N}{2}}{N^2}=\frac{1}{4}$. Interesting at 90 K on heating, the snapshots of **Fig. 12(c)** shows that we recover the same self-organization of the spin states, made of alternate ferromagnetic-like HS and LS stripes as those obtained at 90 K on cooling. On the other hand, the spatial organization of the spin states in the second plateau at 130 K is clearly similar to that obtained on cooling.

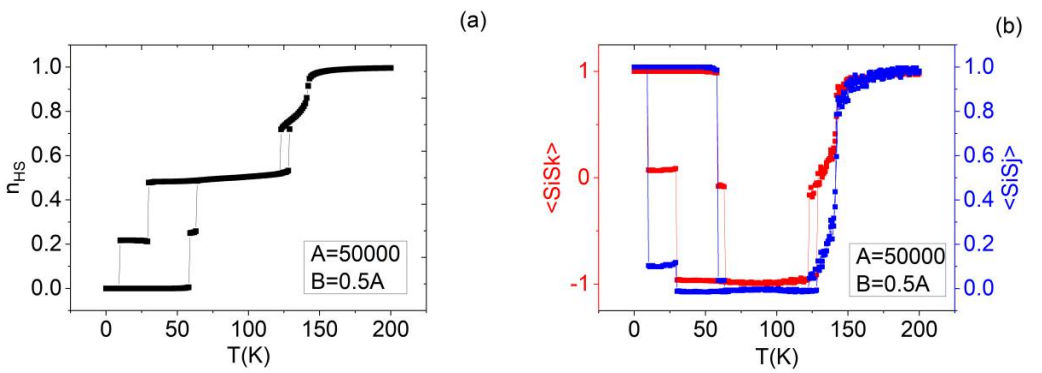

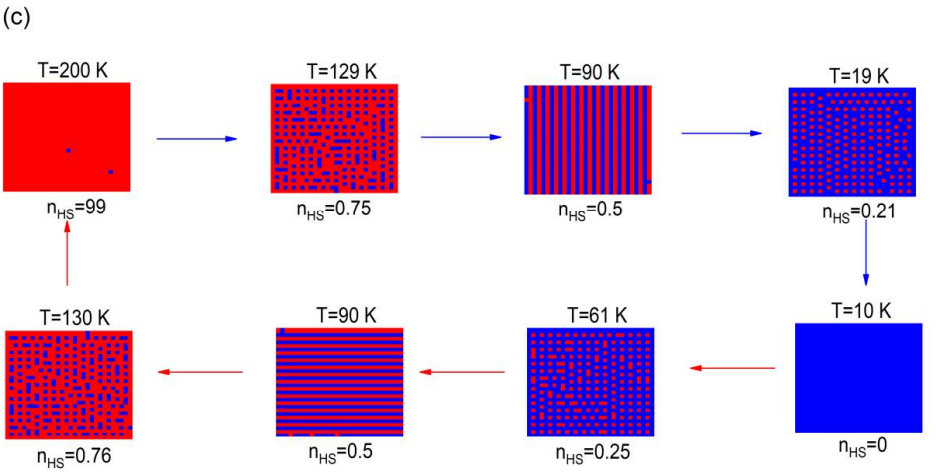

FIG. 12. Thermal-dependence of the (a) HS fraction, n_{HS} and (b) average nn, $< S_i S_j >$ (blue curve) and nnn, $< S_i S_k >$ (red curve), spin-spin correlations, showing three steps transitions made of two first-order transitions and a gradual one. (c) Selected snapshots showing the spatiotemporal organization of the spin states in the plateau regions. Clear self-organizations of HS (red squares) and LS (blue squares) states at $n_{HS} = 0.8$ and 0.5 emerge in the plateaus regions along the heating and cooling processes. The parameter values are the same as those of **Fig. 11(a)**, **(b)** and **(c)** except for nn, $A = 5\ 10^4$ K $\times$ nm^{-2} , and nnn, $B = 0.5 \times A$, elastic constants.

The last simulations in this study concern the case where we break the equality of the energetic contributions between the short-range nn and nnn contributions by taking $A \neq 2B$. So, first, we consider the case, $A = 6\ 10^4$ K $\times$ nm^{-2} and take $B = 0.23 \times A$. Again, the simulations are performed by starting from HS state and then we cool down using the same MC procedure described in Sec. II B. More complex HS to LS thermal transition is obtained, showing four steps transformations where all transitions are of the first-order. Here, all previous plateaus widths appearing at $n_{HS} \sim \frac{1}{4}, \frac{1}{2}$ and $\frac{3}{4}$ are enhanced.

When we start from the HS state, as depicted in **Fig. 13(a)** and **Fig. 13(b)**, a first plateau appears at $n_{HS} \sim 0.8$ with an associated organization of spin states [**Fig. 13(c)**] made of alternate HS stripes and clusters of antiferro HS-LS stripes which appear both along x- and y-directions due to entropy reasons. This leads to several antiphase boundaries, particularly in the center of the lattice. The second plateau is reached on cooling at 87 K. There, $n_{HS} = \frac{1}{2}$, and the self-organization takes place through a checkerboard structure of HS and LS states with some disorder due the existence HS antiphase boundaries made of two nn HS sites which tend to organize along 1D stripes in a ferro-elastic fashion, as clearly depicted by the corresponding snapshot at 87 K. When lowering temperature, the system reaches the third plateau at $n_{HS} \sim \frac{1}{4}$. The spatial organization of the spin states is made of alternate LS stripes and antiferro HS-LS stripes which appear both along x- and y-directions with the some antiphase defects already appeared at 121 K, as shown in the

corresponding snapshot at 39 K. On heating, the HS fraction switches from 0 to $n_{HS} = \frac{1}{4}$ at 64 K, corresponding to the appearance of the plateau. The spatial distribution of the spin states in this intermediate state is shown in snapshot corresponding to $T = 64$ K. One can easily see that this distribution appears as a mirror of that on heating at 115 K, where the ferro HS stripes are now LS. These remarks also apply to the two other plateaus, where the existence of antiferrophase boundaries also appeared.

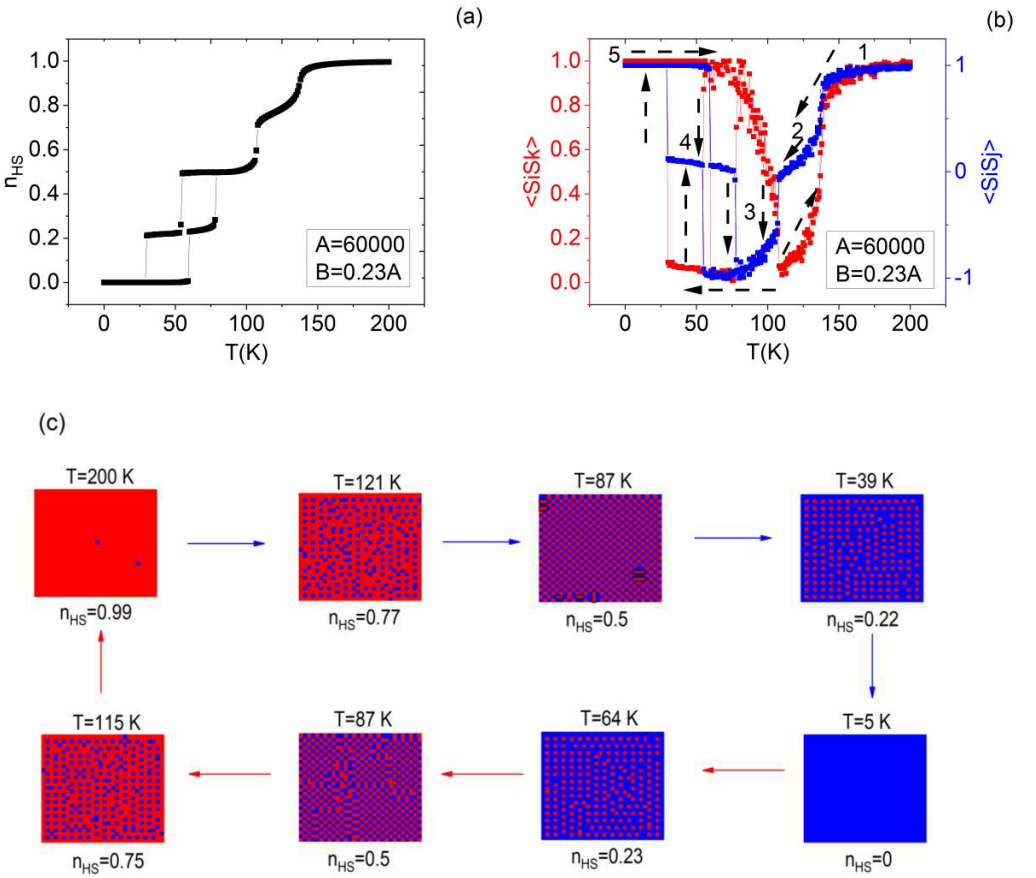

FIG. 13. Thermal-dependence of the (a) HS fraction, n_{HS} and (b) average nn, $< S_i S_j >$ (blue curve) and nnn, $< S_i S_k >$ (red curve), spin-spin correlations, showing four steps transitions made of a gradual transition and three first-order transitions during cooling and heating. (c) Selected snapshots showing the spatiotemporal organization of the spin states in the plateau regions. Clear self-organizations of HS (red squares) and LS (blue squares) states at $n_{HS} = 0.8$, and $n_{HS} = 0.5$ and $n_{HS} = 0.25$ emerge in the plateaus regions along the heating and cooling processes. The parameters values are the same as those of **Fig. 11(a)**, **(b)** and **(c)** except for nn, $A = 6\ 10^4$ K $\times$ nm^{-2} , and nnn, $B = 0.23 \times A$, elastic constants.

By decreasing the value of the elastic constant A and increasing a little bit the ratio B/A, so as to have $A = 5\ 10^4$ K $\times$ nm^{-2} , and $B = 0.28 \times A$, the multistep transition of **Fig. 14(a)** emerges from the simulations, mixing gradual and first-order transitions. In this case, the thermal averages of nn and nnn

spin-spin correlations [**Fig. 14(b)**] exhibit complex behavior, which can be understood by examining the spatial organization of the system along the thermal transition. An important remark relates here with emergence of the alternate HS, LS 1D ferro-structures that we characterized before as an expression of the presence ($T = 90$ K, $n_{HS} = 1/2$) of nnn antiferro interaction [**Fig. 14(c)**]. The re-emergence of these patterns is difficult to predict since the ratio B/A is smaller than in **Fig. 13(a)**, although we decreased the value of the elastic constant A.

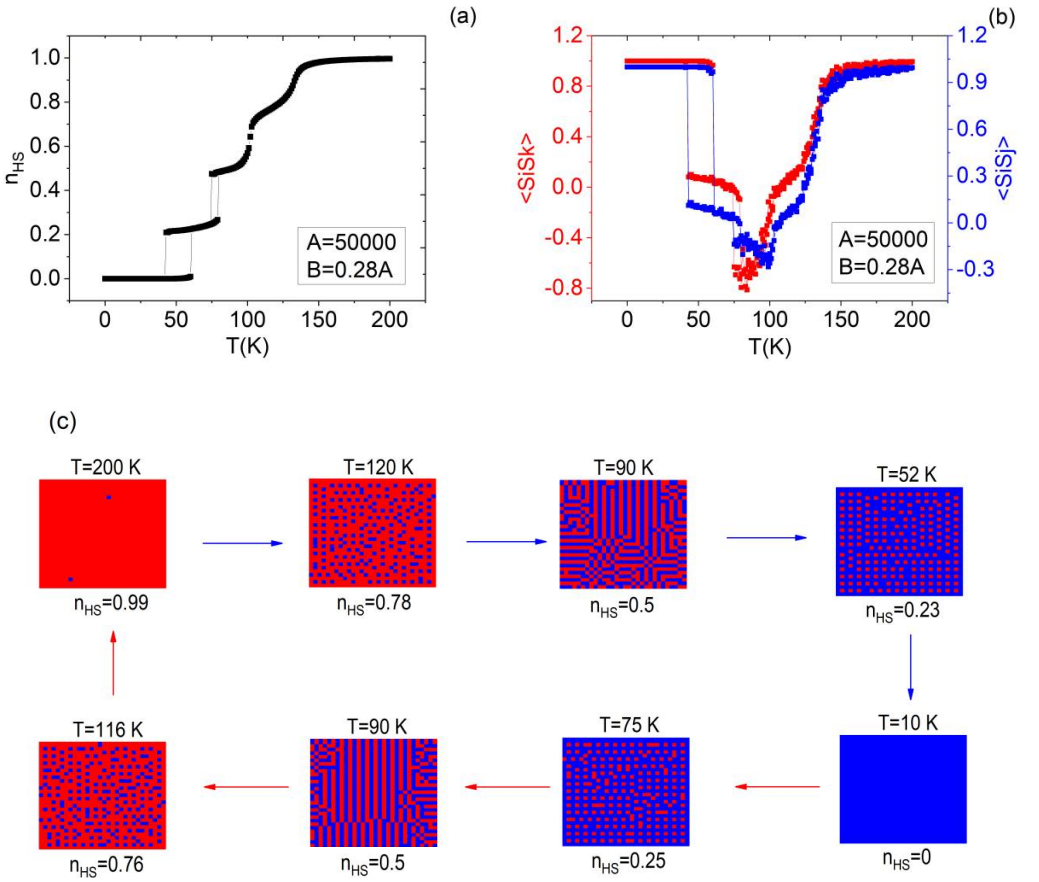

FIG. 14. Thermal-dependence of the (a) HS fraction, n_{HS}, and (b) average nn and nnn spin-spin correlation, $< S_i S_j >$ (blue curve), and $< S_i S_k >$ (red curve), showing four steps transitions made of two gradual and two first-order transitions. (c) Selected snapshots showing the spatiotemporal organization of the spin states in the plateau regions. Clear self-organizations of HS (red squares) and LS (blue squares) states at $n_{HS} = 0.8$, and $n_{HS} = 0.5$ and $n_{HS} = 0.25$ emerge in the plateaus regions along the heating and cooling processes. The parameters values are the same as those of **Fig. 11(a)**, **(b)** and **(c)** except for nn, $A = 5\ 10^4$ K $\times$ nm^{-2} , and nnn $B = 0.28 \times A$, elastic constants.

When we increase the nn and nnn elastic constants, an incomplete phase transition is found when cooling from the HS state [**Fig. 15(a)**]. The high fraction reaches the value $n_{HS} = 0.25$ in low-temperature state.

Compared to **Fig. 14(a)**, the increase of the diagonal elastic constant resulted in the increase of the order in all plateaus regions as well indicated by the average of spin-spin correlations and the lattice snapshots depicted in **Fig. 15(b)** and **Fig. 15(c)**, respectively. In particular, at 90 K and 50 K corresponding to the second plateau ($n_{HS} = 0.5$) nice organized and regular, but incomplete, horizontal HS and LS stripes alternate with the presence of vertical stripes mainly starting from the edges, competing with the previous configuration, which causes the gliding of the chains to each other. On the other hand, the spin organization at 2 K, although similar to that at 75 K on heating of **Fig. 14(c)**, shows a higher level of order with alternating along x- and y-directions of ferro and antiferro chains.

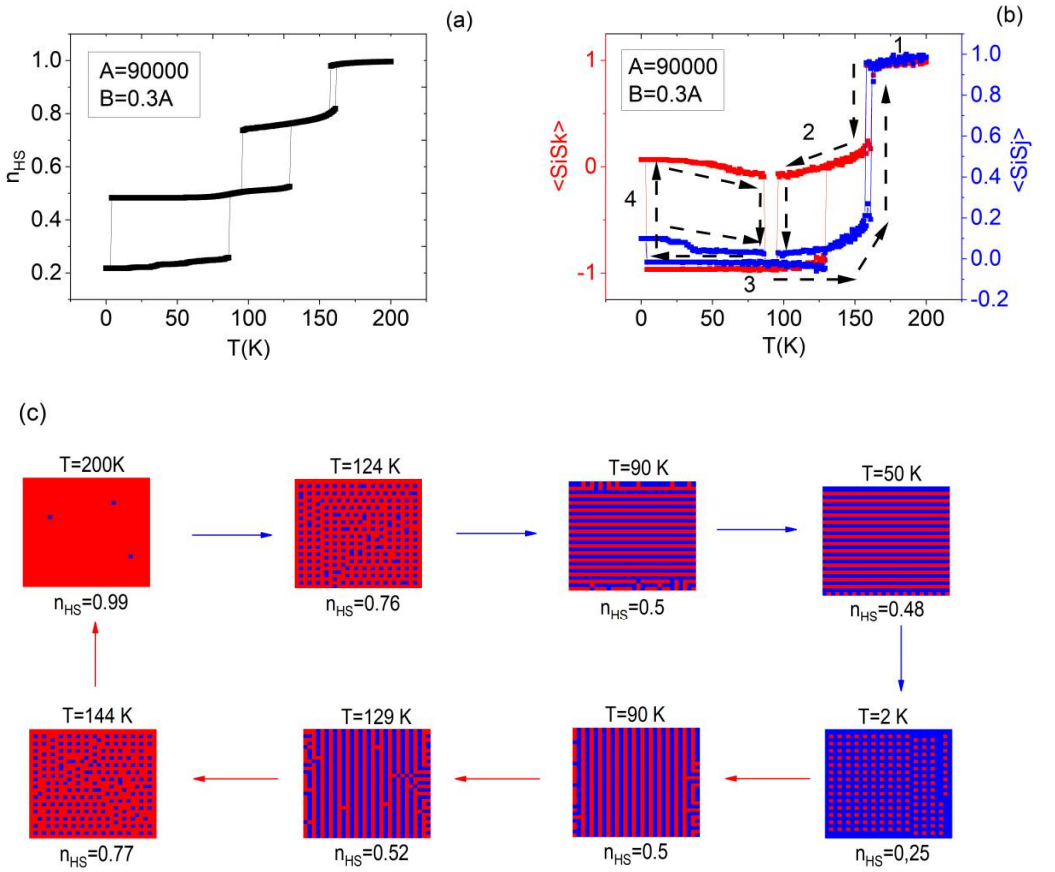

FIG. 15. Thermal-dependence of the (a) HS fraction, n_{HS}, and (b) average nn and nnn spin-spin correlation, $< S_i S_j >$, and $< S_i S_k >$, showing an incomplete three steps corresponding to three consecutive hysteretic 1st order transitions, with a residual low-temperature HS fraction equal to 0.25. (c) Selected snapshots showing the spatiotemporal organization of the spin states in the plateau regions. Clear self-organizations of HS (red squares) and LS (blue squares) states at $n_{HS} = 0.75$, and $n_{HS} = 0.5$ and $n_{HS} = 0.25$ emerge in the plateaus regions along the heating and cooling processes. The parameters values are

the same as those of **Fig. 11(a)**, **(b)** and **(c)** except for nn, $A = 910^4$ K.nm^2 , and nnn, $B = 0.3 \times A$, elastic constants.

IV. CONCLUSION

To conclude, we have studied the thermal and spatiotemporal properties of a 2D spin-lattice system using a homogeneous electro-elastic model. We have shown that starting from the genuine electro-elastic model, in which we considered elastic constants independent of the spin states, and using the approximation of a homogeneous lattice parameter, significantly simplifies the model treatment. Indeed, the mechanical relaxation becomes analytic and the original model transforms naturally to an Ising-like model with long-range ferroelastic and antiferroelastic nn and nnn interactions. Somehow, this homogeneous treatment allows explaining the physical origin of the usual Ising-like model used to describe the thermal properties of SCO materials. In addition, this treatment allowed to identify the elastic origin of the short-range interactions as well as that of the long-range coupling. While the long-range contribution has the tendency to stabilize ordered ferroelastic HS or LS states, the short-range nn and nnn contribution lead to antiferroelastic structures along x- and y-directions, and along the diagonals, respectively. It is interesting to notice that the coexistence of competing long-range ferro-like and short-range nn and nnn antiferro-like interactions generates intrinsic elastic frustration in the lattice, resulting in the impossibility to realize simultaneously antiferroelastic order along the nn and nnn directions. This frustration creates an energetic competition between the elastic energies along x- and y-directions on one hand and along the diagonals on the other. The relevant parameters to control these competing energies are the nn and diagonal elastic constants, whose monitoring led to obtaining a rich variety of thermal behaviors of the high spin fraction, like two- and multi-step transitions (three and four-steps) with complex self-organizations of the spin states in the plateau regions. Among these, organization, checkerboard-like and stripes-like patterns have been obtained. The latter may be constituted of alternate HS or LS ferro-like stripes or alternate ferro (HS or LS) and antiferro-like chains. In this context, this work comes back to the first model one we developed for elastic frustration in SCO materials [89], which also described the occurrence of multistep transitions using a different concept. Finally, this type of treatment opens the way to several extensions, among which the spin-dependence of the elastic constants, the use of anisotropic elastic interactions as well as the use of this model to develop elastic models under pressure for SCO materials. Compared to the usual electro-elastic models, this one presents the advantage of simplicity treatment, since the MC procedure is only applied on the spin states. Finally, it is worth to notice that the number of self-organized structures maybe highly increased if the range of the elastic interactions are increased. In the present study, only nearest neighbors and next-nearest neighbor's elastic interactions are considered, while one can increase this range to further far neighbors. This will increase the rate of frustration in the lattice, which will induce more complex structures and plateaus at the transition. The limiting case being where one considers directional interactions between all lattice sites.

Journal of Applied Physics

AIP Publishing

SUPPLEMENTARY MATERIAL

See the supplemental material for : (i) additional data about self-organization of the spin states of Fig. 9, related to the conditions of obtaining incomplete spin transitions with the presence of complex structures mixing 1D ferroelastic structures along x- and y- directions, and for the evidence of hidden LS states when the simulations are performed by starting from the LS state at low-temperature; and for (ii) the system's phase diagram in the case $B >> A$, corresponding to Fig. 9

DATA AVAILABILITY

The data that supports the findings of this study are available within the article and its supplementary material.

ACKNOWLEDGMENTS

This work was supported by the French-Japan LIA (International Associate laboratory), the ANR project Mol-CoSM N° ANR-20-CE07-0028-02, the Universities of Versailles and Paris-Saclay-UPSAY, and the CNRS (Centre National de la Recherche Scientifique) and the French Embassy in Sénégal. We thank all of them for their financial support.

AUTHOR INFORMATION

Corresponding Author: email: kamel.boukheddaden@uvsq.fr

ORCID

Kamel Boukheddaden: https://orcid.org/0000-0003-0464-1609

Mamadou Ndiaye: https://orcid.org/0000-0001-9370-379X

Houcem Fourati: https://orcid.org/0000-0003-0217-8411

Mouhamadou Sy: https:// orcid.org/0000-0003-2168-4707

Yogendra Singh: https://orcid.org/0000-0002-0049-5512

NOTES

The authors declare no competing financial interest.

Journal of Applied Physics

AIP Publishing

REFERENCES

[1] A. Goujon, F. Varret, K. Boukheddaden, C. Chong, J. Jeftic, Y. Garcia, A.D. Naik, J.C. Ameline, and E. Collet, Inorganica Chimica Acta **361**, 4055 (2008).

[2] S. Decurtins, P. Gütlich, C.P. Köhler, H. Spiering, and A. Hauser, Chemical Physics Letters **105**, 1 (1984).

[3] P. Gütlich, Z. Anorg. Allg. Chem. **638**, 15 (2012).

[4] P. Gütlich, A. Hauser, and H. Spiering, Angew. Chem. **33**, 2024 (1994).

[5] S. Sanvito, Chem. Soc. Rev. **40**, 3336 (2011).

[6] F. Prins, M. Monrabal-Capilla, E. A. Osorio, E. Coronado, and H. S. J. van der Zant, Adv. Mater. **23**, 1545 (2011).

[7] E. Coronado, Nat. Rev. Mater. **5**, 87 (2020).

[8] K. Boukheddaden, M. H. Ritti, G. Bouchez, M. Sy, M. M. Dîrtu, M. Parlier, J. Linares, and Y. Garcia, J. Phys. Chem. C **122**, 7597 (2018).

[9] J. Linares, E. Codjovi, and Y. Garcia, Sensors **12**, 4479 (2012).

[10] J. Zarembwitch and O. Kahn, New J. Chem. **15**, 181 (1991).

[11] O. Kahn and C. Jay-Martinez, Science **279**, 44 (1998).

[12] O. Sato, J. Tao, Y. Z. Zhang, Angew. Chem. Int. Ed. **46**, 2152 (2007).

[13] R. L. Carlin, and A. J. Van Duyneveldt, *Magnetic Properties of Transition Metal Compounds* (Springer, New York, 1977).

[14] O. Kahn, *Molecular Magnetism* (Wiley-VCH: New York, 1993), pp 53.

[15] F. Palacio, *Magnetic Phenomena in Molecular Materials*. In: Coronado E., Delhaès P., Gatteschi D., Miller J.S. (eds) *Molecular Magnetism: From Molecular Assemblies to the Devices*. NATO ASI Series (Series E: Applied Sciences), (Springer, Dordrecht 1996), vol **321**, pp 5–63.

[16] H. Spiering and N. Willenbacher, J. Phys.: Condens. Matter **1**, 10089 (1989).

[17] N. Willenbacher, and H. Spiering, J. Phys. Chem. **21**, 1423 (1988).

[18] H. Spiering, *Elastic Interaction in Spin-Crossover Compounds*. In: *Spin Crossover in Transition Metal Compounds III*. *Topics in Current Chemistry* (Springer, Berlin, Heidelberg), Vol **235**.

[19] K. Boukheddaden, J. Linares, H. Spiering, and F. Varret, Eur. Phys. J. B **15**, 317 (2000).

[20] K. Boukheddaden, J. Linares, and F. Varret, Chemical Physics **172**, 239 (1993).

[21] S.-I. Ohkoshi, K. Imoto, Y. Tsunobuchi, S. Takano, and H. Tokoro, Nat. Chem. **3**, 564 (2011).

[22] T. D. Oke, F. Hontinfinde, and K. Boukheddaden, Eur. Phys. J. B **86**, 271 (2013).

[23] T. D. Oke, F. Hontinfinde, and K. Boukheddaden, Appl. Phys. A **120**, 309 (2015).

[24] T. D. Oke, M. Ndiaye, F. Hontinfinde, and K. Boukheddaden, Eur. Phys. J. B **94,** 38 (2021)

[25] L. Cambi, L. Szegö, and A. Cagnasso, Atti. R. Accad., Naz. Lincei **15**, 266 (1932).

[26] L. Cambi, and L. Malatesta, Ber. Dtsch. Chem. Ges. B **70**, 2067 (1937).

[27] A. Hauser, Coord. Chem. Rev. **111**, 275 (1991).

[28] E. König, Coord. Chem. Rev. **3**, 471 (1968).

[29] P. Gütlich, A. B. Gaspar and Y. Garcia, Beilstein J. Org. Chem. **9342** (2013).

[30] P. J. Van Koningsbruggen, Y. Maeda, and H. Oshio, Iron(III) *Spin Crossover Compounds.* In P. Gütlich, and H. A. Goodwin (Eds.), *Spin Crossover in Transition Metal Compounds I*, *Top. Curr. Chem*. (Springer-Verlag, Berlin, Heidelberg, New York, 2004), Vol. **233**, pp 259–324.

[31] Y. Li, A. Benchohra, B. Xu, B. Baptiste, K. Béneut, P. Parisiades, L. Delbes, A. Soyer, K. Boukheddaden, and R. Lescouzec, Angew. Chem. **132**, 1 (2020).

[32] S. Chorazy, T. Charytanowicz, D. Pinkowicz, J. Wang, K. Nakabayashi, S. Klimke, F. Renz, S-I. Ohkoshi, and B. Sieklucka, Angew. Chem. Int. Ed. **59**, 15741 (2020).

[33] A. B. Gaspar, G. Molnar, A. Rotaru, and H. J. Shepherd, Comptes Rendus Chimie **21**, 1095 (2018).

[34] M. Carmen, J. Muñoz, and A. Real, Coordination Chemistry Reviews **255**, 2068 (2011).

[35] K. Babilotte and K. Boukheddaden, Physical Review B **101**, 174113 (2020).

[36] S. Bonnet, G. Molnar, J. Sanchez Costa, M. A. Siegler, A. L. Spek, A. Bousseksou, W-T Fu, P. Gamez, and J. Reedijk, Chem. Mater. **21**, 1123 (2009).

[37] P. Gütlich, A.B. Gaspar, V. Ksenofontov, and Y. Garcia, J. Phys. Condens. Matt. **16**, S1087, (2004).

[38] M. Sy, D. Garrot, A. Slimani, M. Paez-Espejo, F. Varret, and K. Boukheddaden, Angew. Chem. **128**, 1787 (2016).

[39] A. C. Felts, A. Slimani, J. M. Cain, M. J. Andrus, A. R. Ahir, K. A. Abboud, M. W. Meisel, K. Boukheddaden, and D. R. Talham, J. Am. Chem. Soc. **140**, 5814 (2018).

[40] A. Bousseksou, K. Boukheddaden, M. Goiran, C. Consejo, M. L. Boillot, and J. P. Tuchagues, Phys. Rev. B **65** (2002).

[41] P. Gutlich, Y. Garcia, and T. Woike, Coord. Chem. Rev. **219-221**, 839 (2001).

[42] S. Koshihara, *in Optical Properties of Low-Dimensional Materials*, edited by T. Ogawa and Y. Kanemitsu (World Scientific, Singapore, 1998), Vol. **2**, Chap. 3.

[43] P. Gütlich, and J. Jung, Journal of Molecular Structure **347**, 21 (1995).

[44] J. L. Her, Y. H. Matsuda, M. Nakano, Y. Niwa, and Y. Inada, J. Appl. Phys. **111**, 053921 (2012).

[45] A. Bousseksou, F. Varret, M. Goiran, K. Boukheddaden, J.-P. Tuchagues, *The Spin Crossover Phenomenon under High Magnetic Field. In Spin Crossover in Transition Metal Compounds III*, P. Gütlich, H. A. Goodwin, Eds., *Top. Curr. Chem*. (Springer-Verlag, Berlin, Heidelberg, New York, 2004), Vol. **235**, pp 65–84.

[46] S. Kimura, Y. Narumi, K. Kindo, M. Nakano, and G. Matsubayashi, Phys. Rev. B **72**, 064448 (2005).

[47] Y. Qi, E. W. Müller, H. Spiering, and P. Gütlich, Chem., Phys. Lett. **101**, 503 (1983).

[48] Y. Garcia, O. Kahn, J.-P. Ader, A. Buzdin, Y. Meurdesoif, and M. Guillot, Phys. Lett. A **271**, 145 (2000).

[49] A. Bousseksou, N. Negre, M. Goiran, L. Salmon, J-P. Tuchagues, M-L. Boillot, K. Boukheddaden, and F. Varret, Eur. Phys. J. B **13**, 451 (2000).

[50] T. Mahfoud, G. Molnar, S. Bonhommeau, S. Cobo, L. Salmon, P. Demont, H. Tokoro, S-I. Ohkoshi, K. Boukheddaden, and A. Bousseksou, J. Am. Chem. Soc. **131**, 15049 (2009).

[51] C. Lefter, R. Tan, J. Dugay, S. Tricard, G. Molnár, L. Salmon, J. Carrey, W. Nicolazzi, A. Rotaru, and A. Bousseksou, Chem. Phys. Lett. **644**, 138 (2016).

[52] L-T. Zhang, X-Q. Zhu, S-D. Su, Y-Y. Yang, S-M. Hu, Y-H. Wen, X-T. Wu, and T-L. Sheng, Crystal Growth & Design **18**, 3674 (2018).

[53] S. Xue, Y. Guo, A. Rotaru, H. Müller-Bunz, G. G. Morgan, E. Trzop, E. Collet, J. Oláh, and Y. Garcia, Inorg. Chem. **57**, 9880 (2018).

[54] L. Wiehl, G. Kiel, C. P. Köhler, H. Spiering, and P. Gütlich, Inorg. Chem. **25**, 1565 (1986).

[55] *Spin Crossover in Transition Metal Compounds I-III, Topics in Current Chemistry,* ed. P. Gütlich, H. A. Goodwin (Springer, Berlin, Heidelberg, 2004), Vol. **233–235**.

[56] E. König, *Nature and dynamics of the spin-state interconversion in metal complexes, in Complex Chemistry, Structure and Bonding* (Springer, Berlin, 1991), Vol. **76**, Book Sec.2, pp. 51–152.

[57] P. Guionneau, F. Le Gac, S. Lakhoudi, A. Kaiba, and D. Chasseau, J. Phys.: Condens. Matter **19**, 326211 (2007).

[58] J. Jeftic, F. Varret, A. Hauser, O. Roubeau, M. Matsarski and J.-P. Riviera, Mol. Cryst. Liq. Cryst. **335**, 511 (1999).

[59] C. Chong, A. Slimani, F. Varret, K. Boukheddaden, E. Collet, J-C. Ameline, R. Bronisz, and A. Hauser, Chem. Phys. Lett. **504**, 29 (2011).

[60] Y. Ogawa, S. Koshihara, K. Koshino, T. Ogawa, C. Urano and H. Tagaki, Phys. Rev. Lett. **84**, 3181 (2000).

[61] H. Fourati, E. Milin, A. Slimani, Chastanet, G. Y. Abid, S. Triki, and K. Boukheddaden, Phys. Chem. Chem. Phys. **20**, 10142 (2018).

[62] M. Sy, F. Varret, K. Boukheddaden, G. Bouchez, J. Marrot, S. Kawata, and S. Kaizaki, Angew. Chem. **126**, 7669 (2014).

[63] F. Varret, A. Slimani, K. Boukheddaden, C. Chong, H. Mishra, E. Collet, J. Haasnoot, and S. Pillet, New J. Chem. **35**, 2333 (2011).

[64] K. Boukheddaden and M. Sy, Curr. Inorg. Chem. **6**, 40 (2016).

[65] A. Slimani, F. Varret, K. Boukheddaden, C. Chong, H. Mishra, J. Haasnoot, and S. Pillet, Phys. Rev. B **84**, 094442 (2011).

[66] Z-Y. Li, H. Ohtsu, T. Kojima, J. Dai, T. Yoshida, B. Breedlove, W-X. Zhang, H. Iguchi, O. Sato, M. Kawano, and M. Yamashita, Angew. Chem. **128**, 5270 (2016).

[67] C-J. Zhang, K-T. Lian, S-G. Wu, Y. Liu, G-Z. Huang, Z-P. Ni, and M-L. Tong, Inorg. Chem. Front. **7**, 911 (2020).

[68] M. Castro, O. Roubeau, L. Piñeiro-Lápez, J. A. Real, and J. A. Rodríguez-Velamazán, J. Phys. Chem. C **119**, 17334 (2015).

[69] D. Chiruta, C.-M. Jureschi, J. Linares, Y. Garcia, and A. Rotaru, J. Appl. Phys. **115**, 053523 (2014).

[70] F. Renz, H. Spiering, H.A. Goodwin, P. Gütlich, Hyperfine Interact. **126**, 155 (2000).

[71] S. Bonnet, M. A. Siegler, J. Sánchez Costa, G. Molnár, A. Bousseksou, A. L. Spek, P. Gamez and J. Reedijk, Chem. Commun., 5619 (2008).

[72] P. Gütlich, A. Hauser, and H. Spiering, Angew. Chem., Int. Ed. Engl. **33**, 2024 (1994).

[73] M. M. Dirtu, D. Gillard, A. D. Naik, A. Rotaru, and Y. Garcia, Hyperfine Interact. **205**, 75 (2012).

[74] G. Schwarzenbacher, M. S. Gangl, M. Goriup, M. Winter, M. Grunert, F. Renz, W. Linert, and R. Saf, Monatsh. Chem. **132**, 519 (2001).

[75] K. Boukheddaden, H. Fourati, Y. Singh, and G. Chastanet, Magnetochemistry **5**, 2, 2312 (2019).

[76] Y. Garcia, S. J. Campbell, J. S. Lord, J. Linares, M. M. Dirtu, A. V. Pérez, Y. Boland, V. Ksenofontov, and P. Gütlich, Hyperfine Interact. **226**, 217 (2014).

[77] Z-Y. Li, J-W. Dai, Y. Shiota, K. Yoshizawa, S. Kanegawa, and O. Sato, Chem. Eur. J. **19**, 12948 (2013).

[78] C. Zhang, K. Lian, G. Huang, S. Bala, Z. Ni, and M. Tong, Chem. Commun., (2019).

[79] Y.-X. Wang, D. Qiu, S.-F. Xi, Z.-D. Ding, Z. Li, Y. Li, X. Ren, and Z.-G. Gu, Chem. Commun. **52**, 8034 (2016).

[80] T. Kosone, I. Tomori, C. Kanadani, T. Saito, T. Mochida, and T. Kitazawa, Dalt. Trans. **39**, 1719 (2010).

[81] A. Bousseksou, J. Nasser, J. Linares, K. Boukheddaden, and F. Varret, J. Phys. I **2**, 1381 (1992).

[82] V. Ksenofontov, A. B. Gaspar, V. Niel, S. Reiman, J. A. Real, and P. Gütlich, Chem. Eur. J. **10**, 1291 (2004).

[83]D. Chernyshov, M. Hostettler, K. W. Törnroos, and H-B. Burgi, Angew. Chem. Int. Ed. **42**, 3825 (2003).

[84]E. Trzop, D. Zhang, L. Piñeiro-Lopez, Francisco J. Valverde-Muñoz, M Carmen Muñoz, Lukáš Palatinus, L. Guérin, H. Cailleau, J. A. Real, E. Collet., Angewandte Chemie International Edition, Wiley-VCH Verlag **55**, 8675 (2016).

[85]E. Collet, H. Watanabe, N. Bréfuel, L. Palatinus, L. Roudaut, L. Toupet, K. Tanaka, J.-P. Tuchagues, P. Fertey, S. Ravy, B. Toudic, and H. Cailleau, Phys. Rev. Lett. **109**, 257206 (2012).

[86]S. Pillet, E-E. Bendeif, S. Bonnet, H. J. Shepherd, and P. Guionneau Phys. Rev. B **86**, 064106 (2012).

[87]N. Ortega-Villar, M. C. Muñoz and J. A. Real, Magnetochemistry 2, **16**, (2016).

[88]E. Milin, V. Patinec, S. Triki, E.E. Bendeif, S. Pillet, M. Marchivie, G. Chastanet, and K. Boukheddaden, Inorg. Chem. **55**, 11652 (2016).

[89]M. Paez-Espejo, M. Sy, and K. Boukheddaden, J. Am. Chem. Soc. **138**, 3202 (2016).

[90]Hiroshi Watanabe, Koichiro Tanaka, Nicolas Bréfuel, Hervé Cailleau, Jean-François Létard, Sylvain Ravy, Pierre Fertey, Masamichi Nishino, Seiji Miyashita, and Eric Collet, Phys. Rev. B **93**, 014419 (2016).

[91]K. Boukheddaden, J. Linares, R.Tanasa and C Chong J. Phys.: Condens. Matter **19** 106201 (2007).

[92] A. Slimani, K. Boukheddaden, F. Varret, H. Oubouchou, M. Nishino, and S. Miyashita, Phys. Rev. B **87**, 014111 (2013).

[93] M. Ndiaye, and K. Boukheddaden, Journal of the Physical Society of Japan **89**, 014004 (2020).

[94] J. Cruddas, and B. J. Powell, Inorganic Chemistry Frontiers **7**, 4424 (2020).

[95] J. Cruddas, and B. J. Powell, J. Am. Chem. Soc. **141**, 19790 (2019).

[96] Y. Singh, H. Oubouchou, M. Nishino, S. Miyashita, and K. Boukheddaden Phys. Rev. B **101**, 054105 (2020).

[97] K. Boukheddaden, R. Traiche, H. Oubouchou, and J. Linares, Magnetochemistry **2**, 17 (2016).

[98] M. Nishino, C. Enachescu, and S. Miyashita, Phys. Rev. B **100**, 134414 (2019).

[99] K. Boukheddaden, Phys. Rev. B **88**, 134105 (2013).

[100] C. Jureschi, J. Linares, A. Rotaru, and Y. Garcia, Magnetochemistry **2**, 13 (2016).

[101]K. Boukheddaden, Progress of Theoretical Physics, **112**, 205 (2004).

[102]C. Enachescu, M. Nishino, S. Miyashita, A. Hauser, A. Stancu and L. Stoleriu, Eur. Phys. Lett., **91**, 27003 (2010).

[103]M. Nishino, K. Boukheddaden, Y. Konishi, and S. Miyashita, Phys. Rev. Lett. **98**, 247203 (2007).

[104] J. A. Nasser, K. Boukheddaden and J. Linares, Eur. Phys. J. B **39,** 219 (2004)

[105]W. Nicolazzi, S. Pillet, and C. Lecomte, Phys. Rev. B **78**, 174401 (2008).

[106]W. Nicolazzi, J. Pavlik, S. Bedoui, G. Molnar, and A. Bousseksou, Eur. Phys. J. Spec. Top, **222**, 1137 (2013).

[107] C. Fourmental, S. Mondal, R. Banerjee, A. Bellec, Y. Garreau, A. Coati, C. Chacon, Y. Girard, J. Lagoute, S. Rousset, M-L. Boillot, T. Mallah, C. Enachescu, C. Barreteau, Y. J. Dappe, A. Smogunov, S. Narasimhan, and V. Repain, The J. Phys. Chem. Lett. **10**, 4103 (2019).

[108]C. Enachescu, M. Nishino, S. Miyashita, L. Stoleriu, and A. Stancu, Phys. Rev. B **86**, 054114 (2012).

[109] B. Hôo, K. Boukheddaden, and F. Varret, Eur. Phys. J. B 17, 449 (2000).

[110] T. Nakada, P. A. Rikvold, T. Mori, M. Nishino, and S. Miyashita, Phys. Rev. B **84**, 054433 (2011).

[111] H. Fourati and K. Boukheddaden, Phys. Rev. B **101**, 224101 (2020).

[112] C.P. Slichter, H.G. Drickamer, J. Chem. Phys., **56**, 2142 (1972)

[113] K. Boukheddaden, A. Slimani, M. Sy, F. Varret, H. Oubouchou and R. Traiche, *in Magnetic Structures of 2D and 3D Nanoparticles, Properties and Applications*, ed. J. C. Serge Levy (Berlin, Germany, 2016) chap. 9, p. 333.

[114] A. Bousseksou, G. Molnar, L. Salmon, and W. Nicolazzi, Chem. Soc. Rev. **40**, 3313 (2011).

[115] R. Traiche, M Sy, and K. Boukheddaden J. Phys. Chem. C **122**, 4083−4096 (2018).

[116] W. Selke, Physics Reports (Review Section of Physics Letters) 170, 213 (1988).

[117]D. I. Khomskii, U. Low, Phys. Rev. B **69**, 184401 (2004).

[118]U. Brandt, Z. Phys. B – Condens. Matter 53, 283-287 (1983).

[119] M. M. Ndiaye, S. Pillet, E. E. Bendeif, M. Marchivie, G. Chastanet, K. Boukheddaden, and S. Triki, Eur. J. Inorg. Chem. 305–313 (2018).

[120] T. Boonprab, S. Lee, S. Telfer, K. Murray, W. Phonsri, G. Chastanet, E. Collet, E. Trzop, G. Jameson, P. Harding, and D. Harding, Angewandte Chemie International Edition **58**, 11811 (2019).

[121] H. Fourati, G. Bouchez, M. Paez-Espejo, S. Triki and K. Boukheddaden, Crystals **9**, 46 (2019).

[122] P. Gütlich, V. Ksenofontov and A. B. Gaspar, Coord. Chem. Rev. **249**, 1811 (2005).

[123] A. Hauser, J. Chem. Phys. **94**, 2741 (1991).

[124] K. Boukheddaden, M. Sy, and F. Varret, Adv. Theory Simul. **1**, 1 (2018).